Fast exhumation rate during late orogenic extension: The new timing of the Pilat detachment fault (French Massif Central, Variscan belt)

Véronique Gardien, Jean-Emmanuel Martelat, Philippe-Hervé Leloup, Gweltaz Mahéo, Benoit Bevillard, Pascal Allemand, Patrick Monié, Jean-Louis Paquette, Anne-Sabine Grosjean, Michel Faure, et al.

Fast exhumation rate during late orogenic extension: the new timing of the Pilat detachment fault (French Massif Central, Variscan belt)

Abbreviated title: New timing of the Pilat detachment fault (FMC)

Véronique Gardien*[1], Jean-Emmanuel Martelat[1], Philippe-Herve Leloup[1], Gweltaz Mahéo[1], Benoit Bevillard[2], Pascal Allemand[1], Patrick Monié[3], Jean-Louis. Paquette[4], Anne-Sabine. Grosjean[5], Michel Faure[2], Cyril Chelle-Michou[6], Clémentine Fellah[1]

1: LGL-TPE, CNRS Université Lyon 1/ENS-Lyon, Campus de la DOUA, Villeurbanne, France
2 : Institut des Sciences de la Terre d'Orléans, CNRS-Université d'Orléans, France
3 : Géosciences Montpellier, Université de Montpellier, CNRS, Université des Antilles, Montpellier, France
4: Laboratoire Magmas et Volcans, CNRS, IRD, OPGC, Université Clermont Auvergne, , France
5: Département de Géologie, Université Jean Monnet, UMR6524-CNRS-IRD, Saint-Étienne, France
6: Institute of Geochemistry and Petrology, Department of Earth Sciences, ETH Zürich, Switzerland

*Corresponding author: vgardien@univ-lyon1.fr

Abstract: A leucogranite sill in the footwall of the extensional Pilat shear zone (PSZ) Eastern French Massif Central was emplaced and sheared in a short time interval, between 301.8±3.1 and 303.0±1.6 Ma (zircon U–Pb and mica $^{40}Ar/^{39}Ar$ ages, respectively). Extension ended at 298.5±1.5 Ma ($^{40}Ar/^{39}Ar$ on mica) as shown by a non deformed dike cross cutting the sheared zone. On the hanging wall of the fault, the opening of the St. Etienne Basin filled by coarse clastic sedimentation confirms the existence of a relief south of the PSZ. U-Pb dating of a lithic-rich ignimbrite at the bottom of the basin and of a volcanic layer at the top delivered ages of 310.5±3.4 Ma and 299.3±1.3 Ma, respectively. Close U-Pb and $^{40}Ar/^{39}Ar$ ages from syn- to post-tectonic granites indicate very fast cooling (~150 °C/Myr) and

exhumation rate (6 mm/yr) corresponding to the emplacement of granites in the middle crust immediately followed by their fast tectonic exhumation and cooling into the upper crust. The development of the Pilat fault in the thermally softened crust is responsible for the rapid exhumation of the Velay dome, a Metamorphic Core Complex localized in the footwall of the sheared zone. Here we propose that its rapid exhumation was due to localized sub crustal lithospheric mantle dripping. These new data show that there was only one extensional phase in the PSZ coeval with the opening of the St. Etienne coal Basin. Finally, the new chronology obtained in this study is challenging previous ages suggesting 20 Ma activity for the Pilat shear zone.

Keywords: Variscan belt**,** Pilat shear zone, Velay, lithospheric dripping

1.Introduction

Since 1980 many studies have focused on normal faults observed in continental collision settings (Molnar and Tapponnier, 1977; Malavieille 1993). This has led to the concept of syn- to post-orogenic collapse where normal faults reflect an orogenic scale process that contributes to smooth out the relief: the overthickened, and hence hot and with a low viscosity, crust spreads out, while in the upper crust, the extensional deformation is absorbed on low angle detachment faults above metamorphic core complexes (Wernicke et al., 1987; Malavieille, 1987; Echtler and Malavieille, 1990). To explain such structures, several models invoke either delamination, slab break-off (Sacks and Secor, 1990; Beaumont et al., 2001) or the flow of a partially molten lower crust (Kusznir and Matthews, 1988; Block and Royden, 1990; McKenzie and Jackson, 2002). These tectonic processes accompanying an

elevation of the relief interact with erosion and sedimentation shaping the surface morphology and the relief. To well characterize the extensive context in an orogeny it is necessary to obtain geochronological and structural data. These data would then allow (1) to determine if several extensional events occurred, particularly if ductile deformation were followed by brittle deformation, (2) to place the extension in the magmatic and regional tectonic evolution.

In the French Massif Central it has been proposed that two major events of extensional tectonics occurred successively (Fig. 1A) during the Early Carboniferous (325-315 Ma) and the Late Carboniferous (305-275 Ma) respectively called syn- and post-orogenic extension (Burg et al., 1991; Faure et al., 2009). The Late Carboniferous stage is linked to the formation of several intramontane basins containing abundant clastic deposits with coal intercalations. In this context the St Etienne basin is interpreted as a supra detachment basin above the Pilat low angle shear zone on top of the large Velay granitic dome (Malavieille et al., 1990; Gardien et al., 1997). However, existing geochronological data suggest that the Pilat shear zone is Early Carboniferous in age dated at 322 and 313 Ma (Caen-Vachette et al., 1984; Vitel 1988; Costa, 1990) while structural studies agree with the Late Carboniferous extensive period (Malavieille et al., 1990; Gardien, 1990).

To settle this controversy, we carried out a structural and geochronological study to constrain the deformation in the Pilat shear zone and the timing of sedimentation in the St Etienne basin. Our results allow us to specify if this evolution corresponds to a transient or ending episode of the Variscan orogeny in the French Massif Central.

1.1 Thickening and extensional tectonic episodes in the French Massif Central

The Variscan orogeny (420–300 Ma) results from the collision between Laurussia and Gondwana after the closure by subduction of several oceanic domains (Matte, 1986, 2001; Domeier and Torsvik, 2014; Franke et al., 2017). One of the most metamorphic and thickest parts of the belt crops out in the French Massif Central and in the Armorican Massif. Petrological data imply that the crust reached at least 45 km in thickness (Lardeaux et al., 1989; Gardien et al., 1990) after the collision phase dated at c.a. 360-350 Ma (Gay et al., 1981; Maluski and Monié, 1988, Costa et al., 1993; Gardien et al., 2011; Do Couto et al. 2016; Chelle-Michou et al., 2017) following a subduction phase (Gardien et al., 1988; Mercier et al., 1990). Thereafter, two successive stages of crustal extension affected the French Massif Central during the last stages of its evolution. The first one, during the Early Carboniferous period (Namuro- Westphalian, 325-315 Ma-equivalent to the Serpukhovian of the Internationale Stratigraphic Chart (Gradstein et al., 2012), has been defined based on geochronological and structural data obtained on syntectonic granites and country metamorphic rocks. This stage is characterized by a NW-SE stretching direction in almost the entire French Massif Central (Fig. 1B) (Faure, 1995; Roig et al., 1998; Roig and Faure, 2000; Talbot et al., 2005a, 2005b). At that time compression and transpression were still active in the external parts of the belt (Montagne Noire, Maures-Tanneron, Sardinia) (Lagarde et al., 1994; Feybesse et al., 1995; Carosi and Palmeri, 2002; Rolland et al., 2009; Roger et al., 2015, Trap et al., 2017; Poujol et al., 2017). The second extensional stage occurred during the late Carboniferous-Early Permian period (Stephanian-Autunian, 305-282 Ma equivalent to the Upper Pennsylvanian and lower Cirusalian of the international stratigraphic chart) and is defined as a post collision extension associated with the ascent of migmatitic domes and the opening of Carboniferous intramontane coal basins. Throughout the French Massif Central, this stage is characterized by a NNE-SSW stretching direction (Fig. 1B) (Malavieille et al.,

1990; Malavieille 1993; Burg et al., 1994). However, precise data on how (mode and rate) the relief created during the Varsican orogeny was smoothed are still restricted and imprecise.

1.2 Regional Geologic setting

The St Etienne basin is a ~33 km long trending NE-SW basin filled by continental detrital sediments of Carboniferous age (Fig. 1). The sedimentary succession starts with a coarse-grained breccia and conglomerates locally channelized in a micaceous sandy matrix. These are followed by a mixed well-rounded conglomeratic and sandy sequence with interlayered silts and coal deposits (Becq-Giraudon et al., 1996; Brugier et al., 2003). The plant and spore fossils contained in the coal series of the S^t Etienne basin were used to define the Stephanian stratotype, the continental equivalent of the Moscovian, the Kasimovian, and the basal part of the Gzhelian (Gradstein et al., 2012). To the north the sedimentary series rests unconformably on the metamorphic series of the Mont du Lyonnais while to the south the NE-SW trending St Chamond fault is the basin boundary that separates it from the Pilat Unit (Fig. 1C). The lithology of the Pilat Unit consists of aluminous micaschists, leptynitic gneisses and orthogneisses in which leucogranite pods are variably involved in the main tectonic structures (Malavieille et al., 1990; Gardien 1990). Geochemical analysis indicate that the granites were generated by the partial melting of pelitic sediments (Vitel 1988). The unit underwent a high-temperature and low-pressure metamorphism superimposed on a former medium pressure and temperature metamorphic stage related to a top to the south nappe stacking predating the normal faulting (Gardien 1990; Gardien et al., 1997). The main structure of the Pilat Unit is characterized by a foliation plane mainly parallel to the lithological limits, dipping 5 to 30° to the north (Figs. 1C and 2) and supporting a stretching

lineation trending N160° to N30° (Fig. 1C) dipping of 0 to 30° towards the north (Fig. 2). The foliation plane consists of quartzo-feldspathic layers interbedded with mica-sillimanite rich layers wraping garnet and staurolite relicts and bear a biotite lineation. In the southern part of the Unit, numerous kinematics indicators: S-C plane relationships, shear bands, feldspar asymmetric tails and pressure shadows show top-to-the-north sense of shear compatible with a kilometer-scale normal shear zone: The Pilat Shear Zone (PSZ) (Malavieille et al., 1990). To the south, the Velay granito-migmatitic dome is found at the base of the PSZ (Figs. 1C and 2). At the Gouffre d'Enfer locality a leucogranite sill intrusive in the micaschist is interpreted as synkinematic with the top-to-the-north sense of shear (Malavieille et al., 1990). Its whole rock Rb/Sr date of 322±9 Ma was interpreted as Bashkirian-Moscovian (Namuro-Westaphalien: 325-315 Ma) age of the ductile shearing (Caen-Vachette et al., 1984; Vitel, 1988). Such age was corroborated by a biotite $^{39}Ar/^{40}Ar$ date of 313±6 Ma (Costa, 1990) of a lenticular orthogneiss located in the southern part of the Pilat unit (sample Pl11, Figs 1 and 2). Biotite and muscovite from an aluminous micaschist (sample Pl2) surrounding the lenticular orthogneiss yield dates of 296.0±3.1 and 299.7±3.1 Ma respectively interpreted as the minimum age for the extensional deformation (Costa, 1990). The St Etienne basin, Gzhelian in age (Stephanian: 305-299 Ma) would have opened later, synchronously with the motion of a second detachment that crosscuts the former shear zone hanging wall and connects to the first one at depth (Malavieille et al., 1990). This stage was dated at 290.9±3.1Ma in a granite ($^{39}Ar/^{40}Ar$ on biotite Costa, 1990) crosscut by the St Chamond fault delimiting the St Etienne basin to the south (sample Pl4, Figs 1 and 2). Altogether these geochronological data suggested that the motion of the Pilat fault lasted at least 30 Ma from the ductile deep to superficial brittle stages. Alternatively, Mattauer and Matte (1998) interpret the St Etienne coal basin as a pull apart basin along the right-lateral

St Chamond Fault crosscutting the PSZ. Indeed, based on the previous geochronological data and structural analysis, the model proposed by Mattauer and Matte (1998) proposed that the opening of the Carboniferous basin of St Etienne was dissociated from the activation of the Pilat normal fault. They put forward two stages for the opening of the basin i) a pull apart system which formed on a dextral detachment relay allowing a thick sedimentation in the basin and ii) followed by a compressional stage occurring in its southeastern part and responsible for the deformation within the basin.

2. Material and Method

2.1 Sampling description (Figure 3)

To better constrain the age of the Pilat extensional "system" we have sampled granites and a micaschist from the Pilat Unit (refer to figures 1 and 2 for sample location). We have sampled the previously dated syntectonic leucogranite from the Gouffre d'Enfer (PL06, Figs 3a, b) and complemented with samples from two other granites from the Pilat Unit. These new sample sites are moderately affected (pegmatites PL49 and PL51) and unaffected (microgranite PL43) by extensional tectonics, respectively. Dating the three granites allowed us not only to constrain the duration of the Pilat normal fault but also the magmatic activity associated with the late evolution of the belt. We have selected a plane of a brittle normal fault (PL48) crosscutting a microgranite PL 43 to date the extensional superficial brittle stage. The fault plane contains a mineral stretching lineation down-dip on the fault plane underlined by white mica that are amenable to dating.

To provide the first radio-isotopic age constraints on the volcano-sedimentary series of the St. Etienne Carboniferous Basin we have selected two volcanic samples belonging to the base (PL92) and to the top (PL90) of the sedimentary series (Fig. 1C). One sample (PL90)

corresponds to a cinerite interbedded with coal deposits outcropping at the Ricamary site south of St. Etienne providing a minimum age for the coal basin. The second sample (PL92) is a previously described rhyolitic dyke on the 1/50 000 geological map of St. Etienne (Chenenvoy et al., 1970) outcropping at the base of the basin east of St. Chamond. We have used the U/Pb by LA-ICP-MS method on separated zircons from the granites and the volcanic rocks. We have also selected a micaschist sample south of the St. Chamond fault (PL94) to verify the existence of a second superficial detachment that has been previously proposed as responsible for the opening of the St. Etienne Coal Basin (Fig. 5 in Malavieille et al., 1990). We have used the laser probe $^{40}Ar/^{39}Ar$ method on separated micas from the granites and the micaschist.

2.1.1 The Studied samples

The Gouffre d'Enfer leucogranite (sample PL06) forms a NE-SW oriented sill intruding the southwestern and lower part of the micaschists of the PSZ (Figs. 1C and 2). The leucogranite displays an equant texture free of deformation which passes locally to an orthogneissic or even to a highly deformed rock with a mylonitic texture. The mylonitized zones show an N-S trending lineation (Figs. 3a and d) defined by elongated biotite ± sillimanite crystals hosted by an E-W to N30 oriented foliation plans (Fig. 3e). Shear criteria as feldspar asymmetric tails and S-C plane relationships (Fig. 3b) indicate top to the north sense of shear (Pitiot, 1984; Vitel, 1988; Malavieille et al., 1990). The leucogranite and the micachists display concordant boundaries and tectonic structures as foliation and shear planes (Fig. 3c). Previous structural studies conclude that the leucogranite emplacement is contemporaneous with the regional deformation (Malavieille et al., 1990). The ductile structures are cut by brittle normal faults and sinistral strike-slip faults oriented N45 to N90 (Figs. 2 and 3e). The PL06 sample is

composed of quartz forming ribbons, feldspar, biotite, and muscovite oriented in both S and C planes. The basal and deepest part of the intrusion is marked by the occurrence of sillimanite elongated in the foliation plans and shear bands.

The most southerly collected granite (sample PL43, Fig. 1C and 2) corresponds to a vertical two-mica microgranite dyke cross cutting a migmatitic orthogneiss (Fig. 3f). In the migmatitic orthogneiss (sample PL44) the relationships between the foliation plans and the shear bands indicate a normal motion toward the North (Fig. 3h). The microgranite, made of millimeter size muscovite and biotite associated with quartz, plagioclase, and K-feldspar (Fig. 3g) shows no evidence of ductile deformation. However, the microgranite and the orthogneiss are crosscut by a series of sub-vertical fractures and slip planes with white micas and quartz striations (Fig. 3i). Sample PL48 is one of these fault planes oriented N80, dipping 50° toward the south and bearing N-S elongated white mica dipping toward the south.

We have collected two samples of a pegmatitic leucogranite sill (PL 49 and PL 51) which crops out in the middle part of the Pilat micaschist Unit (Fig. 3j) and whose orientation and dip are subparallel (angular shift from 5° to 10°) to the foliation of the host micaschists (Fig. 3l). The weak deformation affecting the pegmatite is shown by the development of a weak foliation plane emphasized by recrystallized quartz ribbons as well as slight undulose extinctions in muscovite and feldspar porphyroclasts. Late high angle brittle normal faults crosscut the pegmatite (Fig. 3k and m) and the fault planes show striations outlined by quartz and white micas. The orientation and dip of the fault planes as well as the striations indicate a brittle N-S direction of extension (Fig. 3n and o).

Sample PL94 is a micaschist taken from the northern part of the Pilat Unit above the PSZ, near the St. Chamond fault that bounds the St. Etienne Carboniferous basin to the south. The main paragenesis in this sample consists of an association of muscovite + quartz +

feldspars elongated in the foliation plane and surrounding more or less retrogressed garnet and staurolite relicts (Gardien, 1990). Here the foliation is either vertical or dipping 50° to the west, and striking N-S to N20°. The foliation is crossed by different generations of quartz-chlorite veins (Fig. 4a).

Near the city of Grand Croix (Fig. 1), a lithology has been previously described as a rhyolite dyke (1/50000 geological map of St. Etienne, Chenevoy, 1970). We re-sample this unit (PL 92) in the same outcrop and in our view, it does not show a clear dyke crosscutting relationship with the metasediments, but rather consists of blocks of green rocks within a conglomeratic series. Microscopic observations show that the rock is composed of an assemblage of very small quartz grains, pyrophyllite and chlorite replacing a glassy matrix. The latter contains phenocrysts of quartz, plagioclase, and highly altered micas as well as many small fragments (diameter < 0.5 mm) of metamorphic rocks including quartzite and micaschist (Figs. 4b, c and d). Thus, in this work we consider sample PL92 as a lithic-rich ignimbrite rather than a rhyolitic dyke.

A sample of sediments of the St Etienne basin was picked near St. Etienne city. This site exposes stratified sedimentary rocks showing alternations of coal and ash layers. Sample PL90 was taken in an ash layer containing non-altered micas, iron oxides and zircon (Fig. 4e).

2.2. Analytical methods

2.2.1. U/Pb (LA-ICP-MS) on separated zircon

Rock samples were crushed and < 400 µm sieved fractions were processed using a Wilfley shaking table, a Frantz magnetic separator and heavy liquids (methylene iodide) to extract zircons. Zircons grains were handpicked under a binocular microscope, mounted in epoxy and polished to expose their interior. Zircons grains were imaged with cathodoluminescence

(CL) on a JEOL CamScan scanning electron microscope (using a 10 kV accelerating voltage) at the University of Geneva, Switzerland for sample PL06 Appendix 1 (Supplementary data) and at the University of Clermont-Ferrand, France for samples PL92 and PL90.

U-Th-Pb isotope data were measured by laser ablation inductively coupled mass spectrometry (LA-ICP-MS) at the Laboratoire Magmas & Volcans (Clermont-Ferrand, France) using a Resonetics M-50 193 nm Excimer laser system coupled to a Thermo Element XR sector field ICP-MS. Helium carrier gas was supplemented with N_2 for sensitivity enhancement [Hurai et al., 2010; Paquette et al., 2014]. The laser operated with a spot size of 27 µm, a repetition rate of 3 Hz, and a fluence of 2.5 J/cm^2. Reduction of raw data was carried out using the GLITTER® software package (van Achterbergh et al., 2001). Isotope ratios were corrected for laser-induced and instrumental mass fractionation via sample-standard bracketing using the GJ-1 zircon reference material (Jackson et al., 2004). Data were not corrected for common Pb. $^{207}Pb/^{206}Pb$ vs. $^{238}U/^{206}Pb$ diagrams were generated using the Isoplot/Ex v. 2.49 software of Ludwig (2001). 2σ level error ellipses incorporate both internal and external uncertainties. The 91500 (Wiedenbeck et al., 1995) zircon reference material (132 analyses: 1063.9 ± 2.4 Ma) was analyzed along with the samples to independently monitor the external precision and accuracy of the measurements. Detailed analytical data for samples PL06, PL90 and PL92 are given in the Appendix 2 (Supplementary data).

2.2.2. $^{40}Ar/^{39}Ar$ dating on separated micas

Rock samples were broadly crushed, washed, dried, and finally sieved to select the 200-400 µm fraction. Unaltered grains of mica were then carefully sorted under the binocular lens, then cleaned with alcohol and distilled water. The picked micas were irradiated in the TRIGA

reactor of Pavia (Italia) together with several monitors of Taylor Creek sanidine at 28.34 ± 0.28 Ma (Renne et al., 1998). After irradiation, the samples were loaded in a CO_2 laser extraction-purification line connected to a multi-collector mass spectrometer for argon analyses (Argus VI by ThermoFisher at the Montpellier University, France) equipped with four Faraday cups and one CDD multiplier for ^{36}Ar. Argon isotope intensities were acquired simultaneously on the five detectors in ten runs. Air aliquots from an automated pipette system were analyzed each sample to monitor mass discrimination and detector bias. Step-heating degassing of the micas was done by regularly incrementing the laser power to recover the distribution of argon isotopes in the mineral and to reconstruct its age spectrum. For each spectrum, two to five mica grains were simultaneously degassed depending on their size. Ages reported on the spectra have been obtained after correction with blanks, mass discrimination, radioactive decay of ^{37}Ar and ^{39}Ar, irradiation-induced mass interferences and atmospheric contamination. They are reported with two sigma uncertainty and were evaluated using a $^{40}Ar/^{36}Ar$ value of atmospheric argon of 298.6 (Lee et al., 2006) and the decay constants of Steiger and Jäger (1977). Different decay constants have been more recently proposed (Min et al., 2000; Renne et al., 2011) but until now there is no full consensus for their use in $^{40}Ar/^{39}Ar$ dating (Fleck et al., 2019; Schaen et al., 2020). The raw data obtained during the acquisition are processed under ArArCalc (Koppers, 2002) to calculate the ages of the age spectra and isochron plots. A summary of argon results is given in table 1. Detailed analytical data are given in the Appendix 3 (Supplementary data).

The micas collected for dating the rocks were analyzed with a SEM coupled to an EDX at the ENS-Lyon. The chemical composition in mass percentages of biotite and muscovite are comparable to those found in granites. The results of the analyses see Appendix 4 (Supplementary data) reveal a homogeneous chemical composition from the core to the

edge. The Al_2O_3 contents vary from 35 to 38%, the K_2O varies from 10 to 11% and their Si contents are constant (~6.15). The analyzed biotite grains (PL06 and PL43) have an Al2O3 contents which vary from 20 to 23%. Biotite from sample PL43 contain 28% of FeO while biotite from PL06 is poorer in FeO (19%) and richer in MgO (~8%), alkalis (K_2O) vary from 8.5 to 11%. Their Si / Al ratios are homogeneous in the range of 1.6 to 1.8. The maps of element distributions presented in Appendix 4 (Supplementary data) confirmed that the dated biotite and muscovite are not zoned and do not present traces of alteration.

3. Geochronological Results

3.1. U-Pb dates

The Gouffre d'Enfer syntectonic granite (Sample PL06) contains poorly translucent zircons with varied shapes (elongated or rounded). They are composed of inherited relict cores surrounded by oscillatory zoned rims of magmatic origin (Fig. 5; Photo Zr PL06). There is no textural evidence for metamorphic zircon overgrowth. Dating the zircon rims provides two main populations of concordant U-Pb dates at ca. 528 Ma and 301.8±3.1 Ma (lower intercept, n = 14, Fig. 5) respectively. An intermediate group of concordant dates at ca. 470 Ma has also been measured and most likely represents an Ordovician inherited component in the source of the granite.

The volcanic layer (sample PL 90) provided translucent homogeneous needle shape zircons grains with high length to width ratios suggesting rapid growth (Fig. 5). Euhedral grains show oscillatory euhedral zoning consistent with a magmatic origin (Fig. 5). Some crystals display rounded gap growth corresponding to former gas bubble footprints (Zr40, Zr48, and Fig. 5). No inherited relict cores have been identified. Such morphology is consistent with an igneous origin of the zircons. Most points are concordant and yield a lower intercept date of 299.3±1.3 Ma.

The zircon population from the lithic-rich ignimbrite (PL92) is homogeneous, characterized by translucent crystals with potentially corroded and inherited cores (Zr14, Fig. 5) surrounded by thick euhedral oscillatory zoning rims. A wide range of concordant dates are obtained from 850 to 310 Ma as expected for a volcano clastic rock. For such rock type, the emplacement age is constrained by the youngest zircon population defining a lower intercept date of 310.5±3.4 Ma (n = 7). All the youngest dates were obtained on euhedral grains showing oscillatory without any inherited relict cores (grains Zr31, Zr45 and Zr48, Fig. 5).

3.2. $^{40}Ar/^{39}Ar$ ages

It should be noted that all the studied micas provide well defined $^{40}Ar/^{39}Ar$ plateau ages (Table 1 and Fig. 6) for 95 to 100% of the ^{39}Ar released, except for biotite PL43 (Fig. 6 B and C) for which the plateau age was calculated over 60% of the argon release. The intercept ages in the ($^{36}Ar/^{40}Ar$) versus ($^{40}Ar/^{39}Ar$) correlation plot is similar to the plateau ages with atmospheric $^{40}Ar/^{36}Ar$ initial ratios. All experiments show Ca-derived ^{37}Ar close to the detection limit and very low $^{38}Ar_{Cl}/^{39}Ar_K$ values. The biotite grains selected from the syn-kinematic Gouffre d'Enfer granite (PL06) are elongated grains in both foliation planes and shear bands. They yield a plateau age of 303.0 ± 1.6 Ma (Fig. 6A). The white micas selected from the pegmatites (PL 49 and PL51) moderately affected by the shear deformation provided plateau ages of 301.5 ± 1.6 Ma and 302.9 ± 1.6 Ma, respectively (Fig. 6E and F). Muscovite and biotite grains from the post kinematic leucogranite dyke (PL 43) display $^{40}Ar/^{39}Ar$ ages of 298.5 ± 1.5 Ma and 302.9 ± 1.5 Ma respectively (Fig. 6B and C). The elongated white micas on the brittle normal fault plane (PL48) give an age of 303.9± 1.6 Ma (Fig. 6D). Finally, the muscovite grains from the micaschist from the northern part of the Pilat series (PL94) yielded a much older age of 332.8± 1.7 Ma (Fig. 6G).

4. Discussion

4.1. Age of the Pilat Shear Zone motion

U-Pb ages on Gouffre d'Enfer Granite (sample PL06) yield two distinct populations at 530-460 Ma and at 302±3 Ma (Table 2). The two age populations were obtained on distinct crystals; thus, two interpretations are possible: i) It may be considered that the oldest ages may correspond to inherited zircons from surrounding rocks or ii) to the granite source rock, this age being close to the Cambrian age of 545±14 Ma (Rb-Sr method) obtained by Caen-Vachette [1979] on a leptynite from the Pilat Unit. The youngest population may be interpreted as the emplacement age of the granite. However, assuming that the source of Gouffre d'Enfer granite contains zircons of 530-460 Ma, the partial melting of this rock would had probably dissolved some zircons, while other grains included in minerals that are not involved in the fusion reaction would remain intact. The CL images (Fig. 5) show a very dark border around the old zircons, this border too small to be measured can however be synchronous with the youngest zircon population thus we consider that the oldest zircons are inherited from the source of the granite. The 40Ar/39Ar dating of synkinematic biotite for the same rock yields an age of 303.0±1.6 Ma (Table 2) that can receive two different interpretations. It could correspond to the retention of radiogenic argon at temperature of 320-350 °C during the cooling of the granite at relatively fast rates (Harrison et al., 1985). Alternatively, this age could be considered as a crystallization age in agreement with many studies showing that mica ages recorded by deformed rocks are mostly under the control of recrystallization and dissolution/precipitation effects, with a minor influence of volume diffusion processes (Chopin and Maluski, 1982; Di Vincenzo et al., 2004; Augier et al., 2005; Villa, 2014; Bosse and Villa, 2019). However, because the syn-kinematic granite has

emplaced in hot surrounding rocks at temperatures above 700°C, it is likely that the meaning of the biotite age at 303 Ma lies between the two interpretations. The closure temperature in the zircon is considered as ~ 900°C (Cherniak and Watson, 2001), much higher than those of sialic magmas crystallization. We will thus adopt the peak metamorphic temperature at 750-700°C which was recorded by the surrounding metamorphic rocks as the zircon growth temperature. Considering the uncertainties on the ages obtained from the two dating systems, the radiometric data of both chronometers are overlapping. Thus, the cooling between 700°C and 355°C could have occurred either in 2 My or instantaneously. Both hypotheses however indicate that the Gouffre d'Enfer leucogranite experienced a quasi-instantaneous cooling at an average rate of 150 °C/My or more.

The micaschists of the Pilat Unit underwent a low pressure-high temperature (5-6 kbar, 700 °C) metamorphic stage coeval with the development of the PSZ and the emplacement of the syn-kinematic Gouffre d'Enfer granite (stage 2 in the P-T evolution of the Fig. 5 in Gardien, 1990). The granite and the surrounding micaschists were exhumed to the surface before or slightly before the opening of the St. Etienne basin as they are found as blocks in the basal conglomerates of the St Etienne sedimentary basin. Assuming a depth of 18-15 km for the granitic magma emplacement and its final crystallization at 5-7 km in the upper crust as indicated by the presence of retrograde andalusite and pyrophyllite in the micaschists, (stage 3 in the P-T evolution of the Fig 5 in Gardien, 1990) this very rapid cooling is equal to an exhumation rate of ~6 mm/yr. Such result is not incongruous insofar rapid exhumation of deep crustal levels in mountain systems is generally related to extension after thermal softening of a thickened continental lithosphere (Johnston et al., 2000).

The 40Ar/39Ar biotite age of the Gouffre d'Enfer granite is like the biotite age of 302.9±1.5 obtained on the post kinematic leucogranite dyke (PL 43) coming from the

footwall of the fault. Muscovite 40Ar/39Ar ages of 301.5±1.6 Ma and 302.9±1.6 Ma obtained on pegmatititic synkinematic granites (samples PL 49 and PL51 from the PSZ) and of 303.9±1.6 Ma of the lineation of a brittle fault plane (PL48) are statistically similar to the age of the biotite. They are considered to narrowly date their crystallization according to the references cited above showing that white mica ages in crustal scale shear zones are better interpretable to record their (re) crystallization at temperatures up to 550°C. Therefore, these 40Ar/39Ar ages on syn- and post-kinematic biotite and muscovite that crystallized at different crustal levels suggest that the rocks of the Pilat fault footwall were exhumed to the upper crust during a relatively short-lived tectonic event. Muscovite from the post kinematic leucogranite dyke PL 43 gives an age at 298.5±1.5 Ma younger than the biotite age from the same body. This age inversion with respect to the generally assumed closure temperatures of both micas suggests that muscovite could record a crystallization age related to the late infiltration of fluids in the leucogranite along fractures.

The PSZ bordering the northern part to the Velay dome and the granite sills emanating from it (as for example the Gouffre d'Enfer granite) corresponds to the footwall of an extensional fault system allowing the exhumation of the Velay dome. The exhumation of the dome created a relief that was eroded, resulting in coarse-grained clastic sedimentation preserved as boulders in the conglomeratic and brecciated formations at the base of the sedimentary sequence filling the Late Carboniferous basin.

4.2. Relationship between the PSZ and the St Etienne Basin

The basin corresponding to the hangingwall of the fault was filled by sediments comprising very coarse conglomerates and sandstones, including migmatite and granite from the Velay dome and micaschists from the Pilat Unit. The nature of the clasts and their imbrication (Fig. 7) indicate a southern origin confirming that the main relief bordering the

Stephanian coal basin was the Pilat-Velay area. The U-Pb age of 310.5±3.4 Ma obtained on the volcano clastic block (PL92) is compatible with the age Westphalian - Middle Pennsylvanian of the Grand Croix conglomeratic series in which the sample PL92 was taken. This new dating highlights that magmatism in the lower crust responsible for the formation of the granite-migmatite Velay dome and the associated surface volcanism are synchronous with the basin formation whose initiation occurred as early as 310 Ma. The new age confirms that some basins across the French Massif Central could have started to open as early as the Middle Pennsylvanian as for example the Decazeville and the Bosmoreau basins [Bruguier et al., 2003] located along the Sillon Houiller and the Argentat fault respectively (Fig. 1B).

The sedimentary series that have filled the St Etienne basin ended with a fine-grained volcano-detrital sequence alternating with coal layers. The ash sample (PL90) taken at the summit of the series gives a U-Pb age of 299.3±1.3 Ma consistent with the Autunian—Middle Cisuralian age of the surrounding sandstone and shale sediments of the Ricamary site. This age agrees with 297 Ma K–Ar illite age (Bruguier et al., 2003) obtained for the sedimentation in the Carboniferous Bosmoreau basin along the Argentat Fault (Fig. 1B). The St. Etienne coal Basin correspond to an intracontinental rift that opened during Carboniferous time. Whatever the global tectonic context, intracontinental rifting is often synonymous with volcanic activity characterized by the formation of volcanoes in the grabben of the rift, very often related to the astheospheric rise at the base of the thinned crust. Our geochronological data show that the St. Etienne basin begins to open with such magmatic activity as evidenced by the presence of the ignimbrite (PL92) dated at 310 Ma. Between 305 Ma and 300 Ma, extension and magmatic activity were active as indicated by both the emplacement of the syntectonic granite (PL06) from the PSZ and the deposit of the cinerite (PL90) sampled at the top of the sedimentary series of the St Etienne basin. Finally, the

chronological data available before this study were 323 Ma for the Gouffre d'enfer syn tectonic granite (Gay et al.), 313 Ma for an orthogneiss sill in the PSZ and 290 Ma for an undeformed granite (Pl4, Fig. 1) cut off by the St Chamond fault (Costa 1990) suggest a long-lasting activity of the PSZ. This evolution over 20 Ma would therefore comprise two stages, i) an early ductile and deep stage related to the motion of a low angle normal fault (the PSZ) and the exhumation of the Velay granite, ii) a second more surficial stage corresponding to the opening of the Carboniferous basin associated with the development of a second-high angle normal fault connecting in depth to the former ductile fault (Fig. 5d Malavieille et al., 1990). This second fault correspond to the St. Chamont fault which intersects the USG gneiss to the east and surrounded by the Carboniferous basin and the Pilat series to the West (Fig. 1). Our geochronological data are in conflict with such a scheme. Indeed, we have demonstrated the synchronism between the ductile and fragile deformation and thus the opening of the Carboniferous Basin. The St. Chamond fault which limits the basin to the southwest and intersecting the USG gneisses to the east is therefore contemporary with the PSZ further suggesting a single deformation step and potentially a single extensive structure. However, in the absence of a detailed structural study on the fault of St. Chamond, we cannot exclude that the latter is a second fragile and more recent fault superimposed on the PSZ. This could explain the presence of a sheet of coal caught between micachists and controlled by vertical faults bearing horizontal striations showing that these are strike-slip planes (Mattauer and Matte, 1998). Finally, the ages obtained from the PSZ and those of the Carboniferous St Etienne basin suggest that the opening of the basin is coeval with the development of the PSZ contrary to what Mattauer and Matte (1998) proposed.

4.3. Thermal evolution of the crust

4.3.1. Petrological constraints

A common technique to estimate cooling and exhumation rates uses cooling ages from isotopic systems with different closure temperatures. This technique requires the knowledge of the thermal gradient associated with the studied context and be ensured that it remains stable during the exhumation of the rocks. During the continental collision, the Pilat series were buried at a depth of 22-25 km and underwent a prograde metamorphism of medium P and T conditions (8-9 kbar, 650°C; Gardien, 1990). This event occurred before 335 Ma in the Pilat Unit (this study) and between 340 Ma and 360 Ma in the Lyonnais series (Costa et al., 1993) and corresponds to the main nappe stacking event in the eastern part of the French Massif Central. Subsequent evolution under low pressure and high temperature conditions (5-6 kbar, 700-750°C) implies a high thermal gradient of 50°C/km (Gardien et al., 1990; Gardien, 1990) which caused the partial melting of the lower part of the series and the formation of migmatites mainly located to the south and below the Pilat series (Fig. 1 and 2). This partially melted zone gradually becomes toward the south the Velay Dome which consists of migmatites and granites themselves formed at the expense of metapelites and orthogneiss (Downes et al., 1997; Ledru et al. 2001; Barbey et al., 2015) during a high temperature ~ 850 °C and low pressure 4-5 kbar metamorphic stage (Montel et al., 1992; Barbey et al., 1999, 2015). The crystallization of these magmas is dated between 310 and 300 Ma (Barbey et al., 2015; Chelle-Michou et al., 2017).

The peraluminous Gouffre d'Enfer granite (sample PL06) was produced by the melting of pelitic protoliths (Vitel, 1988) and is thought to represent an extension of the Velay dome (Gay et al., 1981; Vitel, 1988). The 302 Ma age of this syn tectonic granite (U-Pb on zircon, this study) clearly shows that the high temperature stage metamorphism was coeval with the northward extensional tectonics of the Pilat Unit. The new zircon U-Pb ages close to the $^{40}Ar/^{39}Ar$ mica ages (303-301 Ma) of the syn-to post-tectonic granites (Samples

PL 49, 51) from the same series characterizes a very rapid cooling of the magmatic rocks during their exhumation.

To test cooling rate of this specific place we performed a 1D thermal modelling of both the footwall (the PSZ) and the hanging wall (The Carboniferous Basin of St Etienne) of the extension area. To do so we will use the geochronological, thermobarometrical and geometrical data of the Gouffre d'Enfer granite emplaced in the footwall of the PSZ.

4.3.2. 1D Thermal modelling (Figure 8)

The thermal evolution of the crust affected by both extension and granite sill intrusion has been estimated from a 1D finite difference model which considers at the surface the possible sedimentation and at depth the latent heat of crystallization of the magma. The heat equation with production and advection terms has been solved classically by a Crank Nicholson scheme (Wilmott et al., 1995) on a grid with 100 m nodes space. We fixed a constant temperature of 0 °C at the top of the crust and the lower boundary of the model is also kept at a constant temperature of 750 °C. Pure shear thinning of the crust is modelled by a linear increase of the upward velocities. The point at the surface has a null velocity. Geochronological and thermobarometrical data (see geochronological results) show that thinning was fast. In less than one My, the granite emplaced between 18 to 15km depth and was exhumed at a depth of 5 km with a velocity around 6mm/ year. To model such average exhumation velocity, an upward velocity of 0.015m/y was set at 18 km depth decreasing linearly to 0 at the surface. The initial geotherm is computed using an internal heat radioactive heat production of 1e-6 W/m^3 and a surface heat flow of 90 mW/m^2 consistent for a thickened crust (Davies & Davies, 2010). The parameters that have been tested are the thickness of the intrusion, the strain rate, and the sedimentation rate.

First, we consider a magma layer of 2 km wide corresponding to the dimensions of the Gouffre d'Enfer granite that intruded instantaneously in the footwall of the fault at a depth of 18 km depth. The intrusion is assumed to be contemporaneous to the crustal thinning and is thus strained during its emplacement. The crystallization of the magma releases heat in proportion to the cooling following equation of Bussod and Williams (1991):

$$\frac{\partial T}{\partial t} = \kappa \frac{\partial^2 T}{\partial z^2} - v \frac{\partial T}{\partial z} + A - H \quad (1)$$

With,T(z) is the temperature at depth z, t is the time, κ is the thermal diffusivity, v is the advective velocity, A is the heat production by radioactivity and H is heat produced by magma crystallization.

$$H = \frac{L}{C(Tl - Ts)} \frac{\partial T}{\partial t} \quad (2)$$

With H = energy of crystallization, L = latent heat of fusion, C = heat capacity, Tl = liquidus temperature, Ts = solidus temperature. Equation (1) is solved by a forward finite difference scheme. The latent heat of crystallization, L, is computed at each time step. The latent heat of crystallization (L) is 28.10^4 J/kg, the solidus temperature (Ts) is 660 °C the liquidus temperature (Tl) is 900 °C and the heat capacity (C) is 1000 J/kg.

4.3.2.1 Results

The results show that when a 2 km thick or wide layer of magma is intruded at 18 km depth at a temperature of 750°C, the magma layer (footwall) crystallizes and cools in less than 500 ky when the crust is not thinned (Fig. 8A). A second case has been tested in which the crust is thinned by pure shear. In this case too, the thermal anomaly produced by the magma is relaxed in less than 500 ky (Fig. 8A). The modelling shows that in both cases (with or without shearing and with or without exhumation) the extremely rapid cooling of a granitic sill is achievable. However, the key point we can learn from the results is that because of the

tightness of the isotherms the thermal field is dominated by the strain effect rather than by the intrusion effect. Thus, the strain effect maintains the crust in hot thermal regime allowing it to flow easily. These results allow us addressing the question of whether the Pilat Shear Zone is a response to the formation of the Velay dome or is consequence. In other words, either the partial melting of the continental crust responsible for the Velay formation has favoured the extensive regime or this extension has induced partial melting of the continental crust by adiabatic decompression. Our numerical modelling is more in agreement with the second hypothesis corresponding to a dominant passive rifting model. To supports this model, we also can invoke the under platting of mantle derived magmas, the so called vaugnerites (Laurent et al., 2017) whose intrusion contemporaneous with the Velay dome formation would have increased the gravitational forces associated with the delamination of the lithosphere under the Velay dome.

4.3.4 High thermal regime, the possible heating sources

The high thermal regime associated with the extensional tectonic in the Pilat Unit showing a widespread melting of the rocks and the formation of anatectic granites has been well tested (Montel et al., 1992; Gardien et al., 1997; Ledru et al., 2001; Laurent et al., 2017). The mechanism classically invoked for such context is the removal of the orogenic root by delamination or rollback (Laurent et al., 2017), inducing a rapid rise of the asthenosphere and a significant heating of the orogenic crust. Consequently, the magmatism is produced by decompression-induced melting of the previously thickened crust and the asthenospheric mantle. This lasting high heat flux after delamination and a very low-density lower crust and mantle maintain the internal part of the Variscan Belt at relatively elevated altitudes with respect to the thickness of the lithosphere. Hence, some authors (Becq-Giraudon et al., 1996) relying on sedimentary structures and paleontological data suggested that at the

period of the extensional tectonics in the Pilat Unit and the opening of the St Etienne Coal Basin the elevation of this part of the belt could have been ~ 4000 m.

4.3.5. Exhumation mechanism

The fast exhumation rates of the Pilat metamorphic Unit and the Velay dome require geological factors including not only a heat source to provide the partial melting of the lower to middle orogenic crust but also driving forces allowing a rock uplift. In that case, the presence of melt in the crust would induce the localisation of strain within shear zones, the latter being a suitable structural geometry able to exhume the deep melted crust. These conditions are present in a scenario involving the removal of part of the lower lithosphere beneath the Velay dome.

Paragneiss and orthogneiss are the dominant constituents of the nappes pile formed during the continental collision at ~345 Ma. They are known to be partially molten during the Carboniferous (345-315 Ma) as evidenced by the formation of migmatites at medium pressure-high temperature conditions (Montel et al., 1992; Ledru et al., 1994; Bé Mézème et al., 2005; Faure et al.,2009; Barbey et al., 2015), to the point of forming plutons like the Tournon granite, the Margueride granite, the Civrieux granite, all dated between 335 and 320 Ma (Laurent et al., 2017 and ref therein). Hence, anatectic domes such as the Velay dome could have developed earlier in the Variscan belt history, especially because extension was already active since the Moscovian. Thus, as such dome appears during the late Carboniferous (Gzhelian), removal of the lithospheric mantle remains, therefore, the most plausible cause of the sudden Pilat/Velay uplift. The Velay a poly-diapir dome corresponds to a multistage emplacement of granites superimposed on extensional structures (Laurent et al., 2017]. During this process, the dome was shifted horizontally southward (Lagarde et al. 1994; Ledru et al., 2001) carrying during its migration rafts of metamorphic units mainly

affected by northward normal fault (Gardien and Lardeaux, 1991; Gardien, 1993; Chelle-Michou et al., 2017). Thus, granites forming the dome intruded the main detachment fault whose ~35 km amplitude (Fig 1A) (Malavieille et al., 1990) and 10 to 30° angle towards the North can accommodate the rise of the dome from 20 km depth.

4.3.6. Thermo-mechanical evolution

Granites and migmatites resulting from partial melting of the continental crust and the lithospheric mantle are abundant in the Variscan chain testifying of the high thermal regime reached during its evolution (Zwart, 1967; Letterrier, 1978; Cuney et al., 1990; Bussien et al., 2008; Von Raumer et al., 2013, Laurent et al., 2017). However, among these plutons very few have the characteristics of domes (i.e., concentric shape of foliations, horizontal structures at the roof progressively tilted to the vertical at its margin, detachment faults bordering the pluton and responsible for is exhumation). The Velay massif has a dome feature (Burg and Vanderhaeghe, 1993; Lagarde et al., 1994; Ledru et al., 2001) reflecting gravitational instabilities that develop at the base of the orogenic crust coeval to the late extensional evolution of the belt (Van den Driesche and Brun, 1992; Gardien et al., 1997; Ledru et al., 2001). The mechanisms invoked for the development of this domes consistently imply lithospheric tear (Ledru et al., 2001; Laurent et al., 2017). Whether it is slab break-off or slab retreat remains an open question. Both mechanisms require that the lithosphere shears horizontally or vertically in its thickness over a large distance. Moreover, the strong coupling between the crust and the lithospheric mantle causing the tearing of the slab affects a wide area in the overriding domain. For example, the tearing of the Indian lithosphere is referred for the formation of MCC North of the Shyok Suture Zone (SSZ) over more than 150 km in the South Karakorum and south Tibet (Rolland et al., 2001). In the

French Massif Central, the very restricted size of the Velay dome (~7000 km2) suggests a punctual removal of the lithospheric mantle such as dripping.

The geochronological data and more precisely the argon ages provide arguments in favour of this localized delamination of the mantle under the Velay. Indeed, the similarity of the micas ages of samples coming from the footwall of the PSZ and from the PSZ itself can be due to a reset of Ar ages even away from the deformation zone due to fluid ingress (Villa, 2014) and metamorphic recrystallization. However, the absence of zonation and retromorphosis on the dated micas grains (see appendix 2) does not argue in favour of resetting the Ar-Ar system in connection with fluid circulation. An explanation for the velocity and synchronism of exhumation on either side of the PSZ is that the lithospheric rebound linked to the mantle dripping provoke the sudden upward of the whole system, including the footwall and the hangingwall of the PSZ. This rebound has the effect of canceling the diachronism of the exhumation between the foot wall and the hanging wall because it is much faster than the exhumation velocity of the Velay along the Pilat detachment fault.

4.3.6.1 Related Evolution of the coal Basin

The effect of sedimentation on the hanging wall of the fault has also been tested. As it concerns the upper crust, only the first five kilometers of the crust have been modelled (fig 8B). At the beginning of the experiment, however, the model was limited to the uppermost 2.5 km of the crust. The velocity field is kept constant and equal to the sedimentation rate except for the first point at the surface for which velocity is nil. The thermal parameters used in the model are given in Table 3.

The effect of sedimentation rate on the thermal state of the upper crust has been tested. Two very small sedimentation rates of 0.005 mm/yr and 0.002 mm/yr, respectively, have

been applied (Fig.8B). The results show that sedimentation has a clear cooling effect on the base of the basin and therefore on the roof of the footwall. Indeed, the base of the basin is at a temperature of 60 °C after sedimentation of 5000 m at a velocity of 5.10-3 m/yr during 1 My while it is only at 40 °C after sedimentation of 2000 m at a velocity of 2.10-3 m/yr during 1 My. The results show that sedimentation has a clear cooling effect at the base of the basin and therefore at the roof of the footwall. Indeed, the base of the basin is at a temperature of 60 °C after sedimentation of 5000 m at a velocity of 5.10 -3 m/yr during 1 My while it is only at 40 °C after sedimentation of 2000 m at a velocity of 2.10 -3 m/yr during 1 My. The modelling shows that the supply of cold material (sediments) on top of the crust prevents the heat diffusion throughout the basin. Thus, a cold thermal gradient prevail in the upper crust (hanging wall) during extension eventually preventing the resetting of the geo chronometers during extensional. The northern part of the Pilat metamorphic series located just below the St. Chamond fault (fig.1) where the basin opened and the sediments were deposited, have preserved the 40Ar/39 Ar age of ~335 Ma that could be assigned to the stacking nappes stacking event during the continental collision

In addition, these results show that independently of the rate of sedimentation, the temperature at the base of the basin remains low precluding thermal degradation of the organic matter (120-200°C). Thus, according to the model, the temperatures obtained during the sedimentation would prevent the formation of coal. It suggests that the formation of the coal layers is not in relation with the formation of the PSZ and the exhumation of Velay. The history of the maturation of the organic matter should therefore be the subject of a specific and detailed study in relation to the history of sedimentation in the basin.

5. Conclusions

The extensional ductile shear zone of the Pilat has been dated through the Gouffre d'Enfer syn-kinematic leucogranite at 301.8 ± 3.1 Ma by U-Pb on zircon and at 303.0 ± 1.6 Ma by the $^{40}Ar/^{39}Ar$ method on biotite.

Argon ages on biotite and muscovite from synkinematic to postkinematic granites from the Pilat shear zone allow the following extensional fault system to be dated from ductile (syn kinematic pegmatites PL 49 and PL51) to brittle (post kinematic leucogranite dyke PL 43 and fault plane PL48) stages between 301.5 ± 1.6 Ma and 303.9 ±1 .6 Ma.

The ages obtained in this study suggest a "rejuvenation" of 20 Ma of the PSZ and thus of the extensional tectonic on the northern border of the Velay Dome connecting it to the generalized Northeast-Southwest Late Carboniferous to Permian extension in the Variscan Belt. By rejuvenating the PSZ we demonstrate that it not a transient extensive episode but the ending extensional phase affecting the Variscan belt. These new geochronological data indicate a very fast cooling and exhumation rates (150 °C/Myr and ~6 mm/yr respectively) of the Gouffre d'enfer granite whose emplacement in the upper crust is due to the motion of the extensional PSZ also responsible for the exhumation of the Velay Dome. We interpret such fast exhumation rate as the result of punctual lithospheric dripping process beneath the Velay dome.

Finally, for the first time we provide absolute ages (U-Pb on zircon) for the opening and filling of the St. Etienne carboniferous basin ranging between 310.5 ± 3.4 Ma (conglomeratic base to the sequence) and 299.3 ± 1.3 Ma (ash layer to the top of the sequence), respectively.

Acknowledgements

This research project was funded by the program SYSTER INSU.

References

Augier R., Agard P., Monie P., Joliver L., Robin C., Booth-Rea G., 2005, Exhumation, doming and slab retreat in the Betic Cordillera (SE Spain): In situ Ar40/Ar-39 ages and P-T-d-t paths for the Nevado_Filabride complex. J. Metam. Geol., 23, 357-381.

Barbey P., Villaros A., Marignac C., Montel JM., 2015, Multiphase melting, magma emplacement and P-T time path in late-collisional context: The Velay example (Massif Central France). Bull. Soc. Geol. France, 186, 2-3, 93-115.

Barbey P., Marignac C., Montel JM., Macaudiere J., Gasquet D., Jabbori J., 1999, Cordierite growth textures and conditions of genesis and emplacement of crustal granitic magmas: The Velay granite complex (Massif Central, France). J. Petrol., 40, 9, 1425-1441.

Beaumont, C.R.A., Jamieson, M.H., Nguyen and Lee, B., 2001, Himalayan tectonics explained by extrusion of a low-viscosity channel coupled to focus surface denudation. Nature 414, 738-742.

Becq-Giraudon, JF., Montenat, C. and Van Den Driessche J., 1996, Hercynian high-altitude phenomena in the French Massif Central: tectonic implications. Palaeogeo. Palaeoclim. Palaeoeco., 122, 227-241.

Bé Mézème E., Faure M., Coherie A., Chen Y., 2005, In situ dating of tectonothermal events in the French Massif belts. Terra Nova, DOI.org/10.1111/j.1365-3121.2005. 00628.

Block, L., and Royden L. H., 1990, Core complex geometries and regional scale flow in the lower crust. Tectonics, 9, 557– 567.

Bosse V., Villa I.M., 2019, Petrochronology and hydrochronology of tectono-metamorphic events. Gondwana Res., 71, 76-90.

Bruguier, O., Becq-Giraudon JF., Clauer, N. and Maluski H., 2003, From late Visean to Stephanian: pinpointing two-stage basinal evolution in the Variscan Belt. A case study from the Mosmoreau Basin (French Massif Central) and its geodynamic implications. Int. J. Earth Sci., 92, 338-347.

Bussien, D., Bussy, F., Masson, H., Magna, T. and Rodionov, N., 2008, Variscan lamprophyres in the Lower Penninic domain (Central Alps): age and tectonic significance. Bull. Soc. géol. Fr., 179, 369-381.

Bussod, G.Y.A. and Wiiliams, D.R., 1991, Thermal and kinematic model of the southern Rio Grande rift: inference from crustal and mantle xenoliths from Kilbourne Hole, New Mexico. Tectonophysics, DOI: 10.1016/0040-1951,91,90051-S.

Burg JP., Vandendriessche J., Brun JP., 1994, Syn-thickening to post-thickening extension-mode and consequences. Compt. Rendus Acad. Sci. Paris, 319, 9, 1019-1032.

Burg JP., Matte P., 1977, Variscan Tectonics and retromorphosis in the Leptino-Amphibolitic series in Hut-Allier and Vallée de la Truyere (French Massif Central). Compt.Rendus Acad. Sci. Paris, 284, 10, 787-790.

Burg JP.and Vanderhaeghe O., 1993, Structures and way upcriteria in migmatites, with application to the Velay dome (French Massif Central). J. Struct. Geol., 15, 11, 1293-1301.

Caen Vachette, M., Gay, M., Peterlongo, J.M., Pitiot, P. and Vitel, G., 1984, Age radiometrique du granite syntectonique du gouffre d'Enfer et du métamorphisme hercynien dans la série de basse pression du Pilat (Massif Central Français). Compt. Rendus Acad. Sci. Paris, 299, 1201–1204.

Caen-Vachette, M., 1979, Age cambrien des rhyolites transformées en leptynites dans la série métamorphique du Pilat (Massif Central français. Compt. Rendus Acad. Sci. Paris, 289, 997-1000.

Carosi, R., & Palmeri, R., 2002, Orogen-parallel tectonic transport in the Variscan belt of northeastern Sardinia (Italy): implications for the exhumation of medium-pressure metamorphic rocks. Geol. Magazine, DOI: 10.1017/S0016756802006763.

Chelle-Michou, C., Laurent, O., Moyen, JF., Block, S., Paquette, JL., Couzinie, S., Gardien V., Vanderhaeghe, O, Villaros, A. and Zeh, A., 2017, Pre-Cadomian to late Variscan odyssey of the

eastern Massif Central, France: formation of the West European crust in a nutshell. Gondwana Res., 46, 170-190.

Cherniak, D.J. and Watson, E.B., 2001, Pb diffusion in zircon. Chem. Geol., 172, 5-24.

Chenevoy M., Perterlongo J.M., Bonte A., Waterlot G., Comte P and de Montjamont M., 1970, Carte Géologique de la France à 1/50 000 Feuille de Saint Etienne, BRGM Orleans.

Chopin C and Maluski H.,1982, Unconvincing evidence against the blocking temperature concept, a reply. Contrib. Mineral. Petrol., 80, 4, 391-394.

Costa S., 1990, De la collision continentale à l'extension tardi-orogénique, 100 Ma d'histoire varisque dans le Massif-Central frnaçais- Une étude chronologique par la méthode 40Ar-39Ar. PhD, Univ Montpellier 2.

Costa, S., Maluski, H. and Lardeaux, J.M., 1993, 40Ar-39Ar chronology of Variscan tectono-metamorphic events in an exhumed crustal nappe: The Monts du Lyonnais complex (Massif Central, France). Chem. Geol., 105, 339-359.

Cuney, M., Friedrich, M., Blumefeld, P., Bourguignon, A., Boiron, M.C., Vigneresse, J.L. and Poty, B. ,1990, Metallogenesis in the French part of the Variscan orogen. Part I: U preconcentrations in pre-Variscan and Variscan formations: A comparison with Sn, W and Au. Tectonophysics, 177, 39-57.

Davis, J.H. and Davis, D.R., 2010, Earth's surface heat flux. Solid Earth, 1, 5-24.

Downes, H., Shaw, A., Williamson, B.J. and Thirlwall, M.F. (1997). Sr, Nd and Pb isotopic evidence for the lower crustal origin of Hercynian granodiorites and monzogranites, Massif Central, France (vol 136, pg 99, 1997). Chem. Geol., 140, 3-4, 289-289.

Do Couto, Da; Faure, M; Augier, R. Cocherie A., Rossi P., Li X., Lin W., 2016, Monazite U-Th-Pb EPMA and zircon U-Pb SIMS chronological constraints on the tectonic, metamorphic, and thermal events in the inner part of the Variscan orogen, example from the Sioule series, French Massif Central. Int. J. Earth Sci., 105, 557-579.

Domeier M, Torsvik TH., 2014, Plate tectonics in the late Paleozoic. Geosci. Front. DOI.org/10.1016/j.gsf.2014.01.002.

Echler, H. and Malavieille, J., 1990, Extensional tectonics, basement uplift and Stephano-Permian collapse basin in a Late Variscan metamorphic core complex (Montagne Noire, southern Massif Central). Tectonophysics, 177, 125–138.

Faure, M. 1995, Late orogenic Carbonife rous extensions in the Variscan French Massif Central. Tectonics, 14, 132–153.

Faure, M., Bé Mézème, E., Cocherie, A., Melleton, J. and Rossi, P., 2009, The South Millevaches Middle Carboniferous crustal melting and its place in the french Variscan Belt. Bull. Soc. Géol. France. 180, 473-481.

Feybesse J.-L., Couturié J.-P., Ledru P., Johan V., 1995, Les granites de la Margeride, de Chambon le Château et de St Cristophe : des laccolites synchrones des derniers stades de l'épaississement varisque. Geol. France, 1, 27-45.

Fleck, Robert J.; Calvert, Andrew T.; Coble, Matthew A.; et al. 2019, Characterization of the rhyolite of Bodie Hills and Ar-40/Ar-39 intercalibration with Ar mineral standards. Chem. Geol., 525, 282-302.

Franke W, Cocks LRM, Torsvik TH., 2017, The Palaeozoic Variscan oceans revisited. Gondwana Res. 48: 257–284. DOI.org/ 10.1016/j.gr.2017.03.005.

Gardien, V, Vanderhaeghe, O., Arnaud, N., Cocherie, A., Grange, M. and Lecuyer, C., 2011, Thermal maturation and exhumation of a middle orogenic crust in the Livradois area (French Massif Central). Bul. Soc. Géol. France. 182, 1, 5-24.

Gardien, V., 1990, Garnet and Staurolite as relictual phases within the LP facies series of the Pilat unit (French Massif Central) - a record of a polyphase tectonometamorphic reequilibration. Compt. Rendus Acad. Sci. Paris, 310, 3, 233-240.

Gardien, V., 1993, Les reliques pétrologiques de haute à moyenne pression des séries du Vivarais oriental (Est du Massif Central français). Compt. Rendus Acad. Sci. Série 2, Mécanique, Physique, Chimie, Sci. univers. Sci. Terre, 316, 1247–1254.

Gardien, V. and Lardeaux, J-M., 1991, Découverte d'éclogites dans la synforme de Maclas : extension de l'unité supérieure des gneiss à l'Est du Massif Central. Compt. Rendus Acad. Sci. Paris. 312, 61-68.

Gardien, V., Lardeaux, J-M. and Misseri, M., 1988, The Monts du Lyonnais peridotites (MCF) – A record of Paleozoic upper mantle subduction. Compt. Rendus Acad. Sci. Paris, II, 307, 19, 1967-1972.

Gardien, V., Lardeaux, J.M., Ledru, P., Allemand, P. and Guillot, S., 1997, Metamorphism during late orogenic extension: insights from the French Variscan belt. Bull. Soc. Géol. France, 168, 3, 271-286.

Gardien, V., Tegyey, M., Lardeaux, J-M; Misseri, M. and Dufour E., 1990, Crust-mantle relationships in the French Variscan Belt: The Example of the southern Monts du Lyonnais Unit. (Eastern French Massif Central). J. Met. Geol., 8, 5, 477-492.

Gay, M., Peterlongo, J.M. and Caen-Vachettte, M., 1981, Age radiométrique des granites allongés et en feuillets minces syntectoniques dans les Monts du Lyonnais (Massif Central français). Compt. Rendus Acad. Sci. Paris. II, 293, 993-996.

Gradstein, F.M., Ogg, J. Schmitz M. and Ogg, G., 2012, The Geologic Time Scale, Elsevier.

Hurai, V., Paquette, J-L., Huraiová, M. and Konečný, P., 2010, Age of deep crustal magmatic chambers in the intra-Carpathian back-arc basin inferred from LA-ICPMS U-Th-Pb dating of zircon and monazite from igneous xenoliths in alkali basalts. J. Volc. Geo. Res.,198, 275-287.

Jackson, S.E., Pearson, N.J., Griffin, W.L. and Belousova, E.A., 2004, The application of laser ablation-inductively coupled plasma-mass spectrometry to in situ U–Pb zircon geochronology. Chem.Geol., 211, 47-69.

Johnston, DH., Williams, PF., Brown, RL., Crowley, JL. Carr SD., 2000, North eastward extrusion and extensional exhumation of crystalline rocks of the Monashee complex, southeastern Canadian Cordillera. J Struc. Geol., 22, 603-625.

Koppers A.A.P., 2002, ArArCALC-sofware for $^{40}AR/^{39}Ar$ age calculation, Computers & Geosciences 28, 5, 605-619.

Kusznir, N. J. and Matthews, D. H., 1988, Deep seismic reflections and the deformational mechanics of the continental lithosphere. J. Petrol., 29, 63–87.

Lagarde, J.-L., Dallain, C., Ledru, P. and Courrioux, G., 1994, Deformation localization with laterally expanding anatectic granites: Hercynian granites of the Velay, French Massif Central. J. Struct. Geol., 19, 839-852.

Lardeaux, JM, Ledru, P, Daniel, I and Duchene, S., 2001, The Variscan French Massif Central—a new addition to the ultra-high pressure metamorphic 'club': exhumation processes and geodynamic consequences. Tectonophysics, 332, 143-167.

Lardeaux, JM., Reynard, B. and Dufour, E., 1989, Kornerupine bearing granulites and post-orogenic decompression of the Lyonnais Mounts (Massif Central, France). Compt. Rendus Acad. Sci. Paris, 308, 16, 1443-1449.

Laurent, O., Couzinie, S., Zeh, A., Vanderhaeghe, O., Moyen, JF., Villaros, A., Gardien, V. and Chelle-Michou C., 2017, Protacted, coeval crust and mantle melting during Variscan late orogenic evolution: zircon U/Pb dating in the eastern French Massif Central. Int. J. Earth Sci. DOI: 10.1007/s00531-016-1434-9.

Ledru, P., Costa, S., Echtler, H., 1994, The massif central : structure. Pre-Mesoz. Geol. France. Relat. Areas, 305–323.

Ledru, P., Courrioux, G., Dallain, C., Lardeaux, J.M., Montel, J.M., Vanderhaeghe, O., Vitel, G., 2001, The Velay dome 2422 (French Massif Central): melt generation and granite emplacement during orogenic evolution. Tectonophysics, 342, 207–237.

Lee, J. Y., K. Marti, J. P. Severinghaus, K. Kawamura, H. S. Yoo, J. B. Lee,and J. S. Kim., 2006, A redetermination of the isotopic abundances ofatmospheric Ar. Geochim. Cosmochim. Acta,70, 4507–4512.

Letterrier, J., 1978, Aspects chimiques des interactions entre les magmas basiques et leur encaissant pélitique dans le plutonisme. Bull. Soc. géol. France, 7, 21-28.

Ludwig, K.R., 2001, User's manual for Isoplot/Ex Version 2.49, a geochronological toolkit for Microsoft Excel. Berkeley Geochronological Center, Special Publication 1a, Berkeley, USA, 55 pp.

Maheo, G., Guillot, S., Blichert-Toft J., Rolland Y. and Pecher A., 2002, A slab breakoff model for the Neogene thermal evolution of South Karakorum and South Tibet. Earth Planet. Sci. Lett., 1995, 45-58.

Malavieille, J., 1993, Late orogenic extension in mountain belts: insights from the basin and range and the late Paleozoic Variscan belt. Tectonics, 12, 5, 1115-1130.

Malavieille, J., Guihot, P., Costa, S., Lardeaux, J.M. and Gardien, V., 1990, Collapse of the thickened Variscan crust in the french Massif central: Mont Pilât extensional shear zone and St Etienne upper Carboniferous basin. Tectonophysics, 177, 139-149.

Malavieille, J., 1987, Extensional shearing deformation and Km-scale-A-type folds in a cordilleran metamorphic core complex (Raft River Mountains, Northwestern Utah). Tectonics, 6, 4, 423-448.

Maluski, H. and Monié, P., 1988, 39Ar/40Ar laser probe multi-dating inside single biotites of a Variscan orthogneiss (Pinet, Massif Central, France), Chem. Geol., 73, 245–263.

Mattaeur, M. and Matte, P., 1998, The St-Etienne Stephanian coal-basin is not the result of a Late-Hercynian overall extension but a pull-apart basin related to a dextral strike-slip fault. Geodyn. Acta, 11, 1, 23-21.

Mattauer M., Brunel M Matte P., 1988, Normal ductile faults again thrusts-Another similarity between the Himalayas and the Varsican Belt of the Frech Massif Central. Compt. Rendus Acad. Sci. Paris, 306, 671-676.

Matte, P., 1986, Tectonics and plate tectonics model for the Variscan belt of Europe. Tectonophysics, 126, 329-374.

Matte, P., 2001, The Variscan collage and orogeny (480–290 Ma) and the tectonic definition of the Armorica microplate. Terra Nova, 13, 122–128.

McKenzie, D. and Jackson, J., 2002, Conditions for flow in the continental crust. Tectonics, DOI: 1010.1029/2002TC001394.

Mercier, L., Lardeaux, J.M. and Davy, P., 1990, On the tectonic significance of retrograde P-T-t paths in eclogites of the French Massif Central. Tectonics, 10, 131-140.

Molnar P and Tapponnier P., 1977, Relation of the tectonics of eastern China to the India-Eurasia collision: Application of slip-line field theory to large-scale continental tectonics. Geology, 5, 4, 212-216.

Montel, J.M, Marignac, C, Barbey, P and Pichavant, M., 1992, Thermobarometry and granite genesis: the Hercynian low-P, high T Velay anatectic dome (French Massif Central). J. Metam. Geol., 10, 1-15.

Min, K., Mundil, R., Renne, P. R., and Ludwig, K. R., 2000, A test for systematic errors in 40Ar/ 39Ar geochronology through comparison with U/Pb analysis of a 1.1-Ga rhyolite. Geochim. Cosmochim. Acta., DOI.org/10.1016/S0016-7037(99)00204- 5.

Paquette, J.L., Piro, J.L., Devidal, J.L., Bosse, V. and Didier, A., 2014, Sensitivity enhancement in LA-ICP-MS by N2 addition to carrier gas: application to radiometric dating of U-Th-bearing minerals. Agilent ICP-MS journal, 58, 4-5.

Poujol, Marc; Pitra, Pavel; Van Den Driessche, Jean; et al., 2017, Two-stage partial melting during the Variscan extensional tectonics (Montagne Noire, France) Conference: Conference on Variscan

Belt - Correlations and Plate Dynamics Location: Rennes, FRANCE Date: 2015.Int. J. Earth Sci., 106, 2, 477-500.

Pitiot P., 1984, Relations des ensembles cristallins du Lyonnais et du Pilat du point de vue structural. Thèses 3ème cycle. Univ Lyon1. 185p.

Renne, PR; Swisher, CC; Deino, AL; et al., 1998, Intercalibration of standards, absolute ages and uncertainties in Ar-40/Ar-39 dating. Chem. Geol., 145, 1-2, 117-152.

Renne, P R.; Balco, G; Ludwig, K R.; et al., 2011, Response to the comment by W.H. Schwarz et al. on "Joint determination of K-40 decay constants and Ar-40*/K-40 for the Fish Canyon sanidine standard, and improved accuracy for Ar-40/Ar-39 geochronology" by PR Renne et al. (2010). Geochem. Cosmochem. Acta, 75, 17, 5097-5100.

Roig, J.Y. Faure, M. and Truffert, C., 1998, Folding and granite emplacement inferred from structural, strain, TEM, and gravimetric analyses: The case study of the Tulle antiform, SW French Massif Central. J. Struct. Geol., 20, 1169–1189.

Roig, J.Y. and Faure, M., 2000, La tectonique cisaillante polyphasée du Sud Limousin (Massif central français) et son interprétation dans un modèle d'évolution polycyclique de la chaîne hercynienne. Bull. Soc. Geol. France, 295–307.

Rolland, Y., Corsini, M., & Demoux, A., 2009, Metamorphic and structural evolution of the Maures-Tanneron massif (SE Variscan chain): evidence of doming along a transpressional margin. Bull. Soc. Geol. France, 180, 3, 217-230.

Rolland, Y., Mahéo, G., Guillot, S., & Pêcher, A., 2001, Tectono-metamorphic evolution of the Karakorum Metamorphic complex (Dassu–Askole area, NE Pakistan): exhumation of mid-crustal HT–MP gneisses in a convergent context. J. Metam. Geol., 19, 6, 717-737.

Rosenberg, C.L., and M.R. Handy., 2005, Experimental deformation of partially melted granite revisited : Implications for the continental crust. J. Metam. Geol., DOI:1111/j.1525–1314.2005.005555. x.

Schaen A., Jicha B., Hog=dges K., et al., 2021, Interpreting and reporting Ar-40/Ar-39 geochronology data. Geol. Soc. Of Am. Bull., DOI : 10.1130/B35560.1.

Steiger RH, Jäger E., 1977, Subcomissionon Geochronology-Convetion on use of decay constantrs in geochronology and cosmochronology. Earth Planet. Sci. Lett., 3, 36, 359-362.

Talbot J.Y., Chen Y., Faure M., 2005b, Pluton-dykes relationships from AMS and microstuctural studies in a Variscan granite from French Massif Central. J. Geophys. Res., 110, B12106.

Talbot, J.Y., Faure, M., Chen, Y. and Martelet G., 2005a, Pull apart emplacement of the Margeride granitic complex (French Massif Central). Implications for the Late evolution of the Variscan orogeny. J. Struct. Geol., 27, 1610–1629.

Trap P, Roger F., Cenki-tok B., Paquette JL., 2017, Timing and duration of partial melting and magmatism in the Variscan Montagne Noire gneiss dome (French Massif Central). Int. Jour. Earth Sci., DOI : 10.1007/s00531-016-1417-x.

Van Achterbergh, E., Ryan, C.G., Jackson, S.E. and Griffin, W.L., 2001, Data reduction software for LA-ICP-MS. Laser ablation-ICP Mass Spectrometry. J. Earth Sci., 29, 239-243.

Villa, I. M., 2014, Diffusion of Ar in K-feldspar: Present and absent. Geol. Soc.London, Special Publications, 378, 1, 107-116.

Vitel, G., 1988, Le granite du Gouffre d'Enfer (Massif Central français) Pétrologie d'un marqueur tectonique Varsique. Bull. Soc. Géol. France, 6, 907-915.

Von Raumer, J.F., Finger, F., Veselá, P. and Stampfli, G.M., 2013, Durbachites–Vaugnerites – a geodynamic marker in the central European Variscan orogen. Terra Nova, DOI: 10.1111/ter.12071.

Wernicke, B.P., Christiansen, R.L., England, P.C. and Sonder, L.J., 1987, Tectonomagmatic evolution of Cenozoic extension in the North America Cordillera. In: Coward, M.P., Dewy, J., Hancock, P.L. (Eds.), Continental Extensional Tectonics. Geol. Soc. London, Special Publication, 28, 203– 221.

Wiedenbeck, M., Allé, P., Corfu, F., Griffin, W.L., Meier, M., Oberli, F., von Quadt, A., Roddick, J.C. and Spiegel, W., 1995, Three natural zircon standards for U-Th-Pb, Lu-Hf, trace element and REE analyses. Geostandards Newsletters, 19, 1-23.

Wilmott, P., Howison, S., Dewynne J., 1995, The Mathematics of Financial Derivatives: A Student Introduction, Cambridge University Press.

Zwart, H.J., 1967, The duality of orogenic belts. Geol. En Mijnb. 46, 283–309.

Figure captions

Figure 1 **A**: The French Massif central in France. The black arrows represent the Namuro-Westphalian extension oriented NW-SE, the red arrows represent the Carboniferous-Early Permian extension oriented NNE-SSW **B**: Location of the main Carboniferous and Permian basins in the French Massif Central. 1 = St Etienne basin, 2= Decazeville Basin, 3 = Bosmoreau Basin. AF = Argentat Fault, SHF = Sillon Houiller Fault. Kinematic of the extensional Namurian Westphalian (black arrow) and Stephanian Early Permian (red arrow) stages, C: Geological and structural map of the Pilat series and of the St Etienne coal basin. A-B and C-D are the cross sections in figure 2. Location of the studied samples together with the radio-chronological available ages in black (this study) and in red (Costa, 1990).

Figure 2: Northwest-Southeast oriented sections (located in Fig 1C) across the St Etienne coal basin, the Pilat metamorphic series and the Velay migmatitic dome, PSZ: Pilat shear Zone. Location of the studied samples. Note the red arrows for PL90, PL92 and PL4. Indeed, those samples are not localized on the trajectory of the cross-sections, they were reported by projection on the cross-section AB for PL90 and PL4 and, on the cross-section BC for PL92, to report their position with respect to the PSZ and the other dated samples.

Figure 3: Outcrop view of the syntectonic Gouffre d'Enfer granite (PL06) **a**: northward mineral lineation (biotite/sillimanite) on the foliation plane, **b**: Plane-polarized optical image of the granite showing the foliation plane / shear band relationship, **c**: Gouffre d'Enfer leucogranite intrusive in the micaschists, **d** and **e**: Schmidt stereonet, lower hemisphere, of foliation/lination and fault/striation data in the Gouffre d'Enfer leucogranite **f**: Outcrop view of the microgranite dyke (PL43) crosscutting migmatitic orthogneiss and **g**: cross-polarized optical image of the microgranite, **h:** Plane-polarized optical image of the migmatitic orthogneiss showing the foliation plane / shear band relationship, **i**: Outcrop view of the migmatitic orthogneiss **J,k, l, m:** Outcrop view of the pegmatitic granitic sill (PL49) cross cut by brittle normal faults; **n** and **o**: Schmidt stereonet lower hemisphere of the schistosity (S) and fault data in the pegmatitic sill PL49.

Figure 4: a) Outcrop view of the northern micaschists series PL94 crosscut by Quartz-chlorite vein; **b**, **c** and **d**: Crossed polarized optical image and details of the rhyolite sample (PL 92); **e**: Crossed polarized optical image of the cinerite (PL 90). Qtz = quartz, Mus = muscovite, Bio = biotite, Plg = plagioclase, ves = vesicle.

Figure 5: LA-ICPMS zircon U-Pb dating results from the Pilat Unit samples. a) Tera-Wasserburg diagrams of the dated zircons from the Gouffre d'Enfer granite (sample PL06), b) representative zircon CL-images for each dated sample and the position of the SHRIMP spot is highlighted. C) Tera-Wasserburg diagrams of the dated zircons from the cinerite (sample PL90), d) representative zircon CL-images for each dated sample and the position of the SHRIMP spot is highlighted. e) Tera-Wasserburg diagrams of the dated zircons from the ignimbrite (sample PL92), f) representative zircon CL-images for each dated sample and the position of the SHRIMP spot is highlighted.

Figure 6: Argon ages for granites and micaschist samples from the Pilat Unit. A: biotite age spectrum

of the granite PL06; B: biotite age spectrum of the microgranite dyke PL43, C: Muscovite age spectrum of the microgranite dyke PL43; D: Muscovite age spectrum of sample PL48; E: Muscovite age spectrum of the pegmatitic granite sill PL49; F: Muscovite age spectrum of the pegmatitic granite sill PL51; G: Muscovite age spectrum of the micaschist PL94.

Figure 7: Rose diagrams of the river current directions from pebble imbrications of the conglomerate in the basal sediments, from cross sections 1 (A) and 2 (B) localized in figure 1.

Figure 8(A): Cooling of a magmatic intrusion at 18km depth with an initial temperature of 750 °C, one geotherm each 50ky; left) without thinning of the crust. The thermal anomaly is less than 0.5 Myr; right) with a pure shear thinning of the crust (strain rate of 4. 10^{-12} s^{-1}), the thermal anomaly is also less than 0.5 Myr. What is dominant on the thermal field is the strain effect more than the intrusion. (B): Thermal evolution of the upper crust with sedimentation effects. The sedimentation has a clear cooling effect by bringing cold sediment at the top of the basin. Left) The base of the basin is at a temperature of 60°C after a sedimentation of 5000m at a velocity of 5. 10^{-3} m/yr during 1 Myr and right) at a temperature of 40°C after a sedimentation of 2000m at a velocity of 1.10^{-3} m/yr during 1 Myr. These temperatures are incompatible with coal formation comprises between 150°C and 200°C.

Tables captions

Table 1: Synthesis of the Ar-Ar ages obtained on the Pilat samples.

Table 2: Synthesis of the ages obtained on the Pilat samples.

Table 3: Thermal data used in the numerical simulation.

Supplementary Data

Appendix 1 : cathodo-luminescence pictures of the zircons from Gouffre d'Enfer syntectonic granite (sample PL06)

Appendix 2a : U-Pb zircon data set of PL06 Gouffre d'Enfer syntectonic granite ; 2b : U-Pb zircon data set of samples PL90 and 92 respectively a cinerite and an ignimbrite from the carboniferous basin of St. Etienne.

Appendix 3 : Detailed argon data of the biotite from samples PL06 and PL43, of the muscovote from samples PL43, PL48, PL49, 51 and, PL94.

Appendix 4 : Composition map and punctual analyzes of the micas dated in this study.

Figure

Click here to access/download;Figure;fig. 1 gardien et al., 2021.pdf

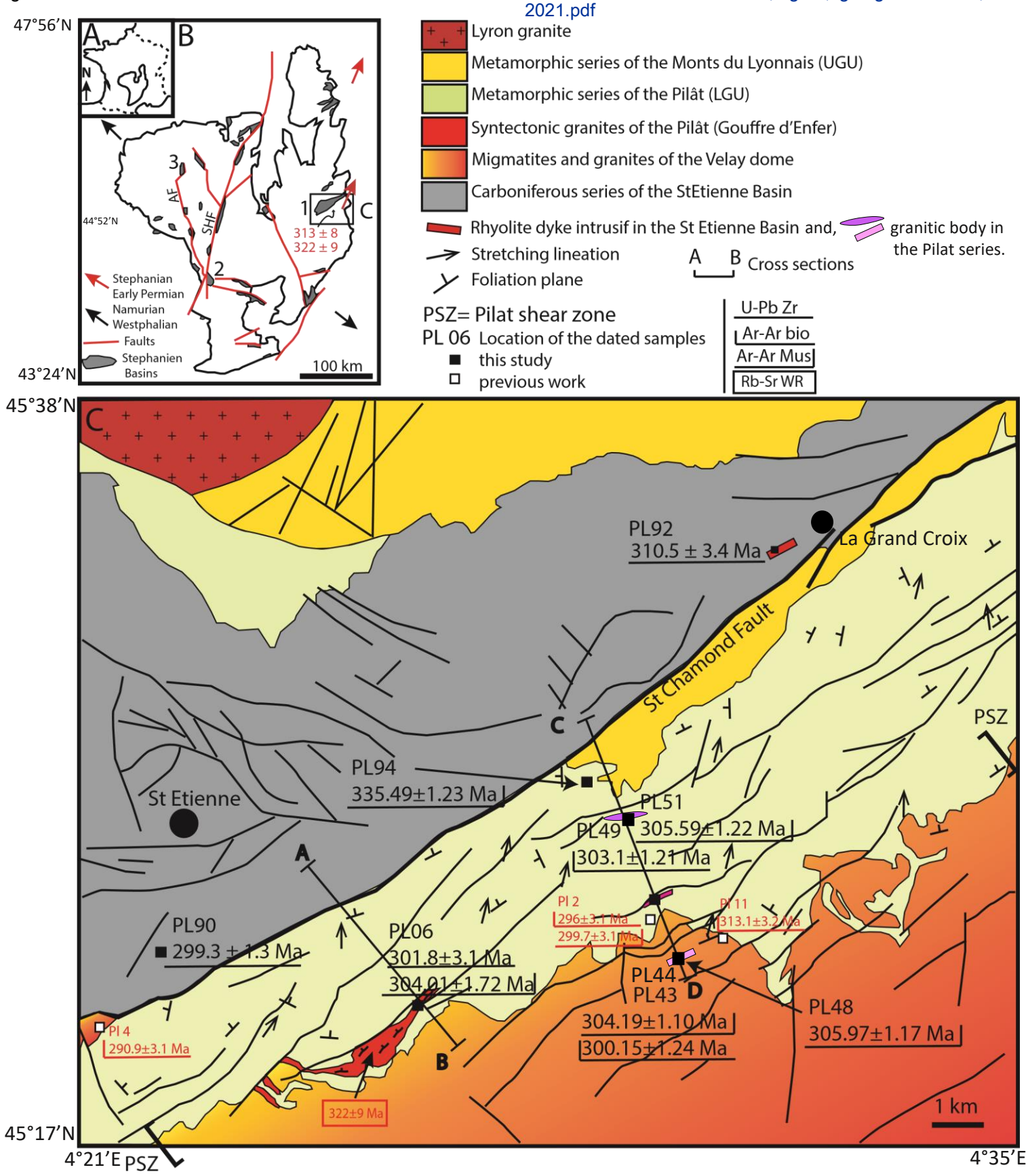

Fig. 1

Figure

Click here to access/download;Figure;fig. 2 gardien et al 2021.pdf

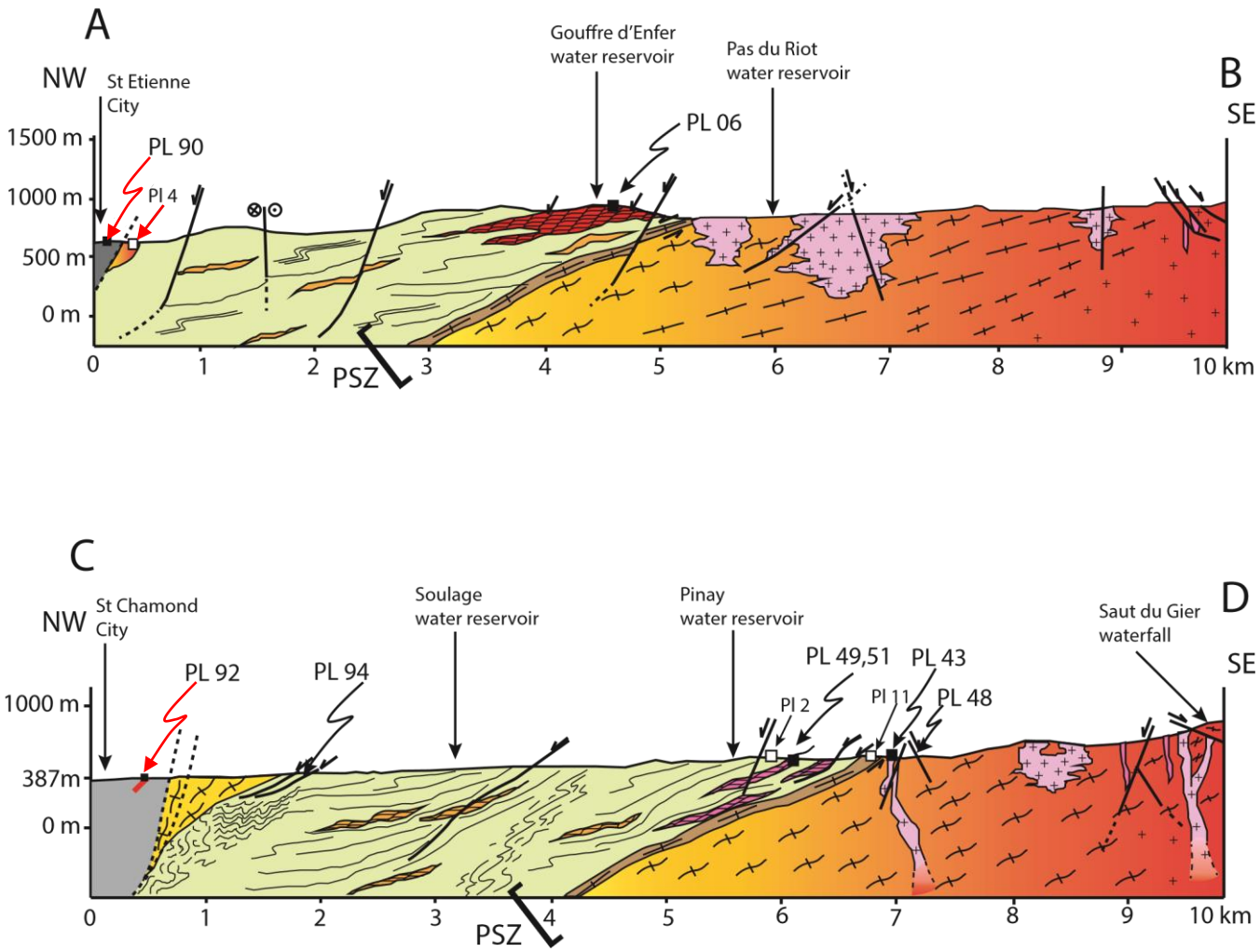

Fig. 2

Figure

Click here to access/download;Figure;Fig. 3 gardien et al., 2020.pdf

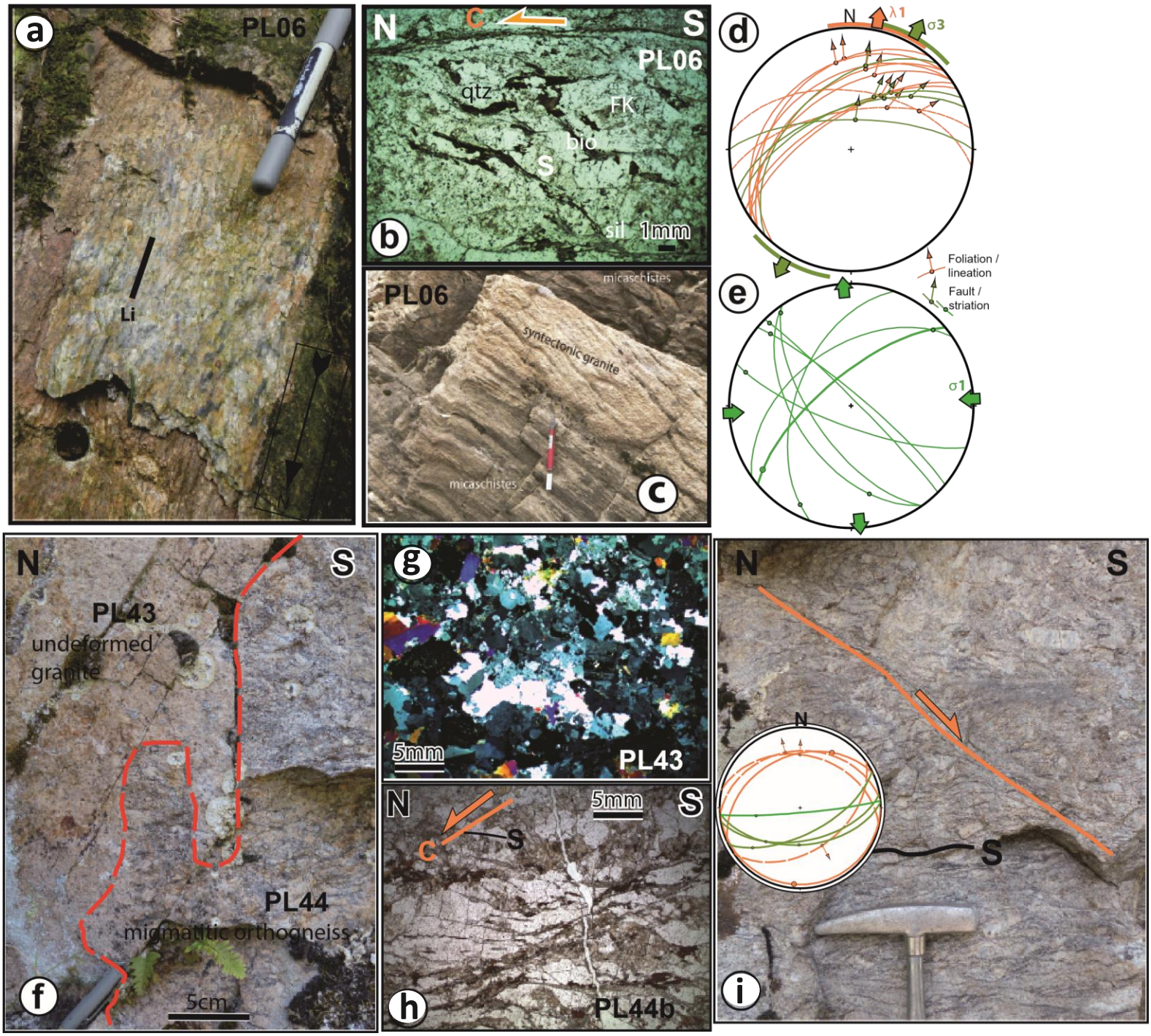

Figure 3

Figure

Click here to access/download;Figure;fig. 3 gardien et al., 2020 (to be continued).pdf

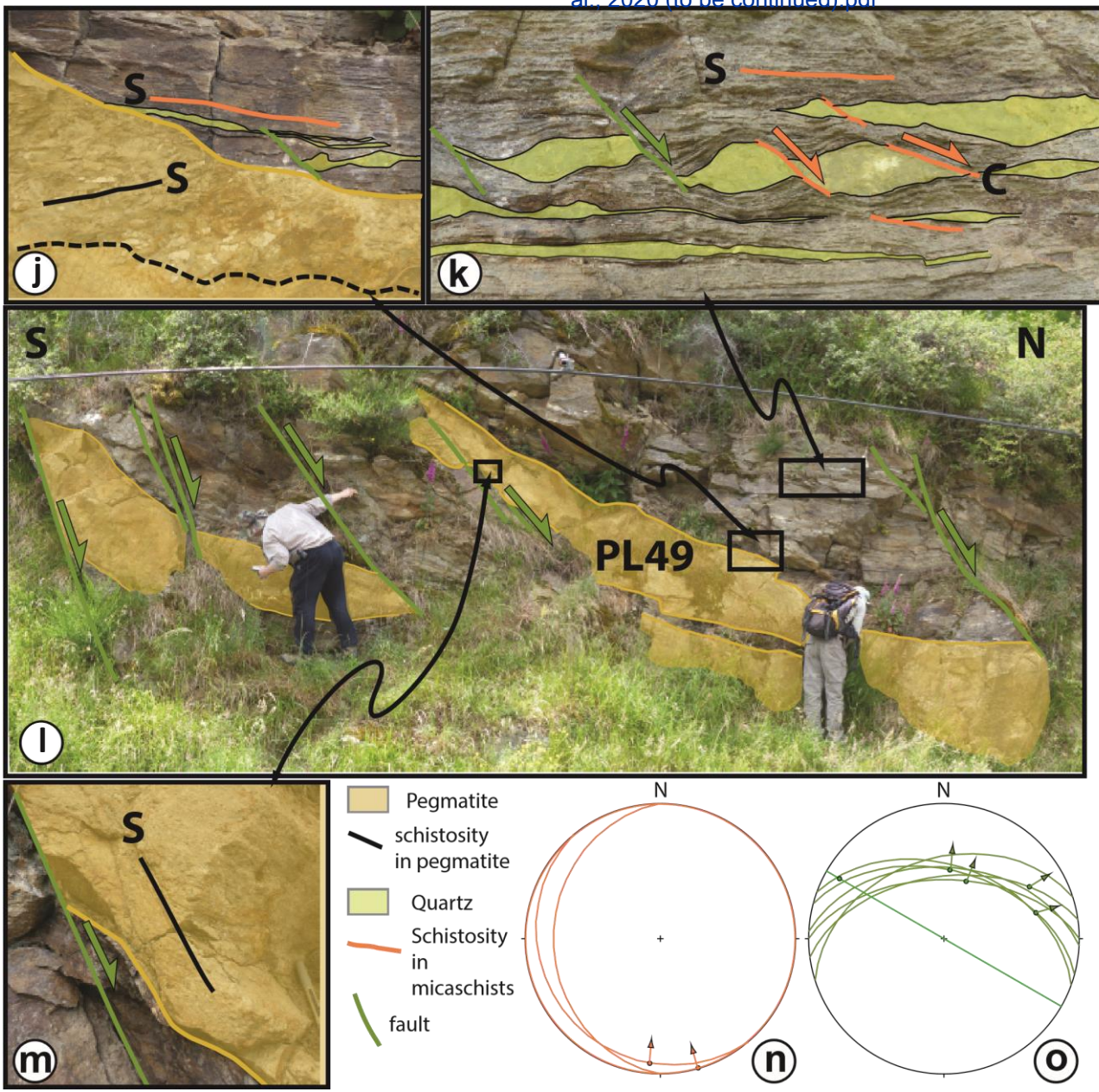

Figure 3 (to be continued)

Figure

Click here to access/download;Figure;fig. 4 gardien et al., 2021.pdf

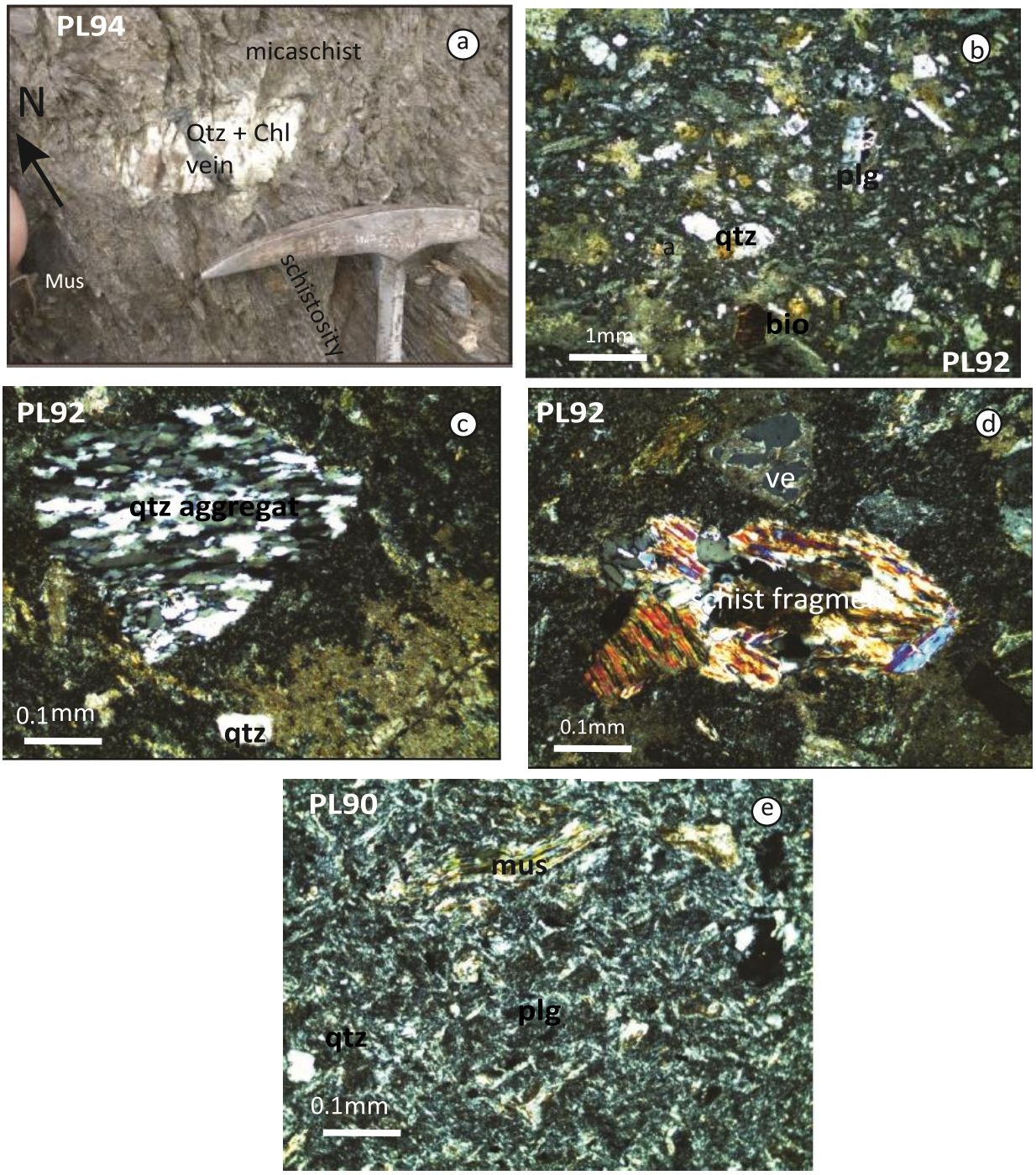

figure 4

Figure

Click here to access/download;Figure;fig. 5 gardien et al 2020.pdf

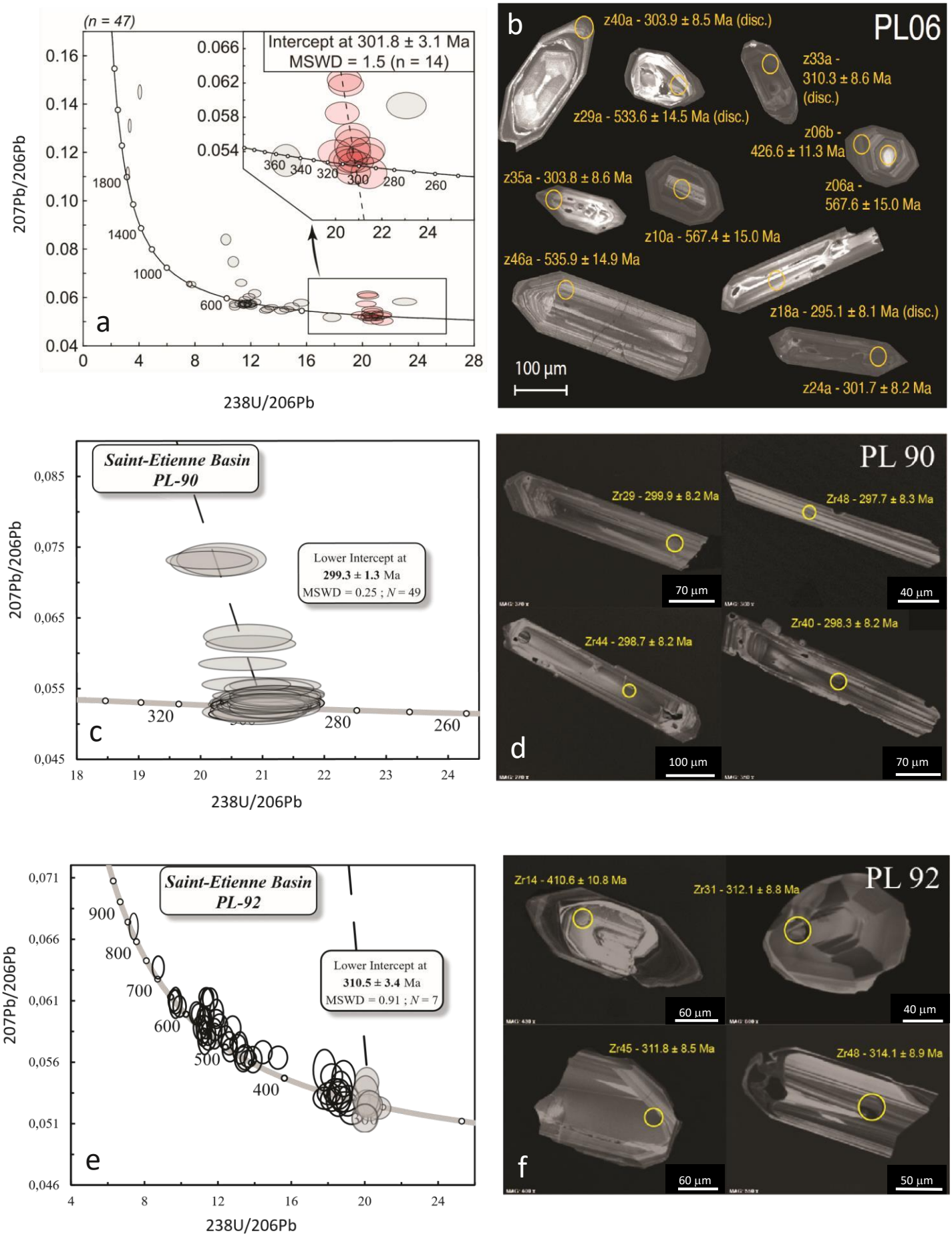

Figure 5

Figure

Click here to access/download;Figure;Fig. 6 gardien et al 2020.pdf

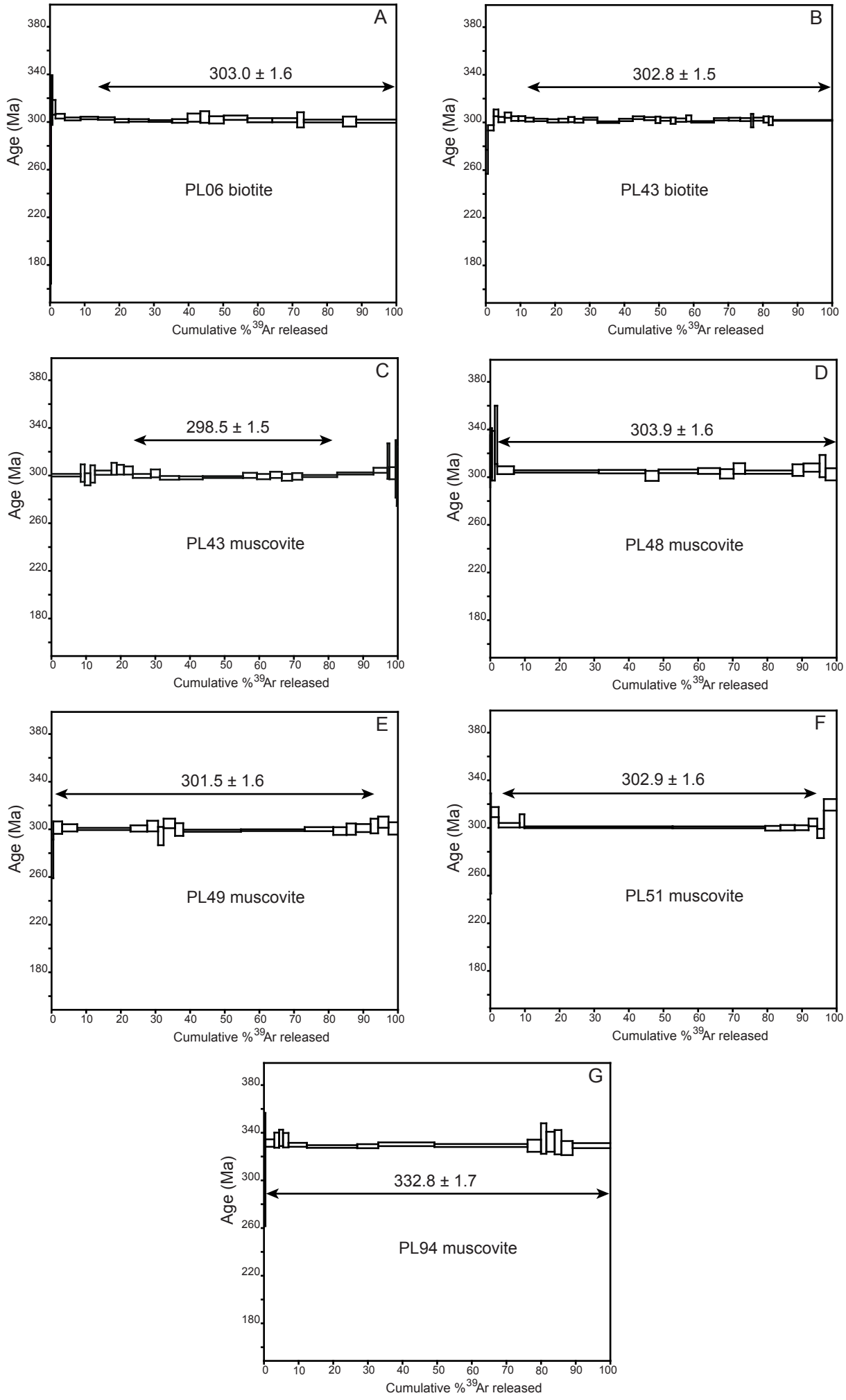

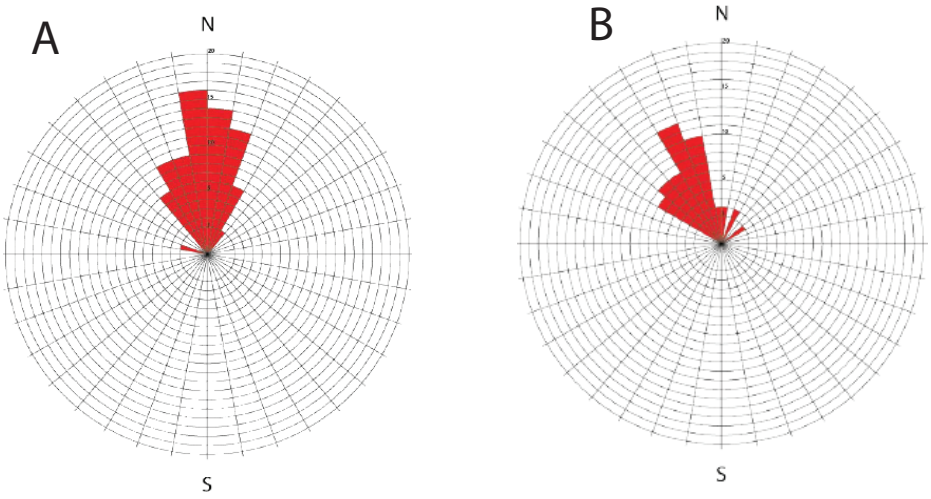

Figure 7

Figure

Click here to access/download;Figure;fig. 8 gardien et al 2020.pdf

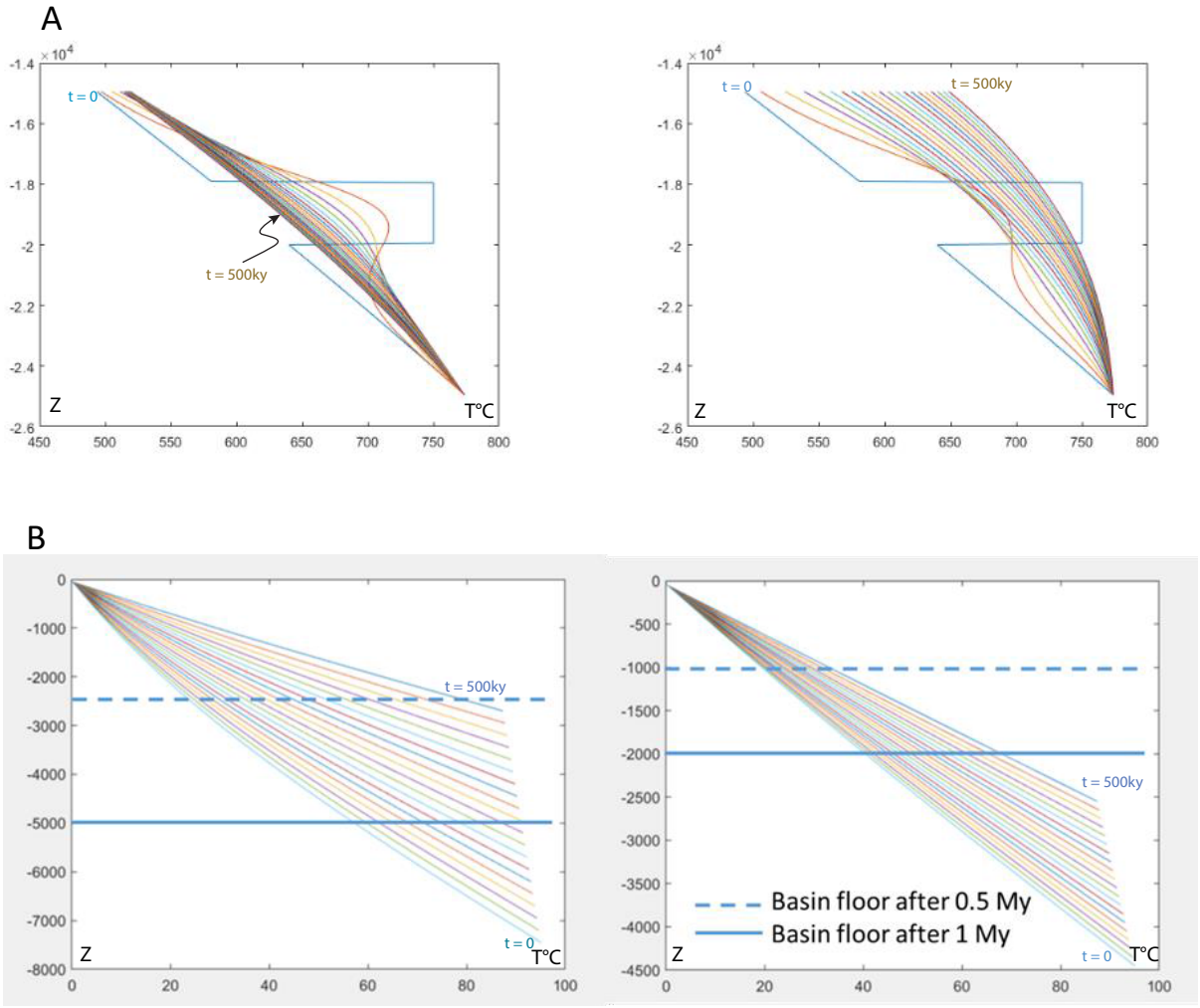

Figure 8

Sample	Total gas age	Plateau age	%39 Ar (steps)	MSWD	Intercept age	40Ar/36Ar	MSWD
PL06 bio	303.1 ± 1.6	303.0 ± 1.6	86.2 (8-22)	1,6	302.9 ± 1.2	300 ± 24	1,74
PL43 bio	302.7 ± 1.5	302.9 ± 1.5 *	88.6 (8-32)	3,25	302.3 ± 1.3	350 ± 70	3,17
PL43 mus	299.8 ± 1.5	298.5 ± 1.5	58.7 (9-19)	1,24	297.5 ± 2.3	373 ± 142	1,25
PL48 mus	303.9 ± 1.6	303.9 ± 1.6	97.5 (5-17)	1,02	303.1 ± 1.3	398 ± 183	1,10
PL49 mus	301.9 ± 1.6	301.5 ± 1.6	93.8 (2-16)	1,58	301.4 ± 1.2	302 ± 5	1,52
PL51 mus	303.8 ± 1.6	302.9 ± 1.6	92.0 (3-10)	2,05	302.6 ± 1.1	304 ± 6	0,99
PL94 mus	333.1 ± 1.7	332.8 ± 1.7	100 (1-16)	1,14	332.6 ± 1.3	306 ± 16	1,28

Table 1

Sample	Locality	Latitude	Longitude	Facies	Mineral	Method	Age (Ma)	±
PL06	Gouffre d'Enfer	45.395008°	4.447512°	Deformed leucogranite	Zircon	U/Pb	301.8	3.1
					Biotite	Ar/Ar	304.01	1.72
PL43	Saut du Gier	45.399960°	4.548759°	Undeformed granite	Biotite	Ar/Ar	304.19	1.1
					Muscovite	Ar/Ar	300.15	1.24
PL48	Scie du Bost	45.399960°	4.548759°	Fault plane	Muscovite	Ar/Ar	305.97	1.17
PL49	Moulin de Cezignieux	45.419400°	4.529815°	Weakly deformed pegmatite	Muscovite	Ar/Ar	303.01	1.21
PL51	Moulin de Cezignieux	45.419400°	4.529815°	Weakly deformed pegmatite	Muscovite	Ar/Ar	305.59	1.22
PL90	La Ricamarie	45.415652°	4.371722°	Cinerites	Zircon	U/Pb	299.3	1.3
PL92	La Grand-Croix	45.506422°	4.565688°	lithic-rich ignimbrite	Zircon	U/Pb	310.5	3.4
PL94	Marie de Châteauneuf	45.322053°	4.385608°	Micaschists	Muscovite	Ar/Ar	335.49	1.23

Table 2

k	thermal conductivity, 2.5 W/m/°
ρ	rock density, 2800kg/m^3
c	heat capacity of rocks, 1400 J/kg
χ	thermal diffusivity of rocks, 1. 10^{-6} m/s^2
A	internal heat production by radioactivity, 1.10-^{6} W/m^3
Q	surface heat flow, W/m^2
C	latent heat of crystallization, 280. 10^3 J/kg
Tl	liquidus temperature, 900°C
Ts	solidus temperature, 700°C

Table 3